Branched Amphiphilic Peptides Capsules for RNA Delivery: Design, Synthesis, and Optimization

by

Collin Christopher Wall

A thesis submitted to the Graduate Faculty of
Auburn University
in partial fulfillment of the
requirements for the Degree of
Master of Science

Auburn, Alabama
May 10, 2025

Keywords: Nanoparticles, RNA, Peptide Synthesis.

Approved by

Adriana Avila-Flores, Associate Professor of Biological Sciences
Alexey Petrov, Associate Professor of Biological Sciences
Katherine Rush, Assistant Professor of Biochemistry

Abstract

RNA is a versatile biomolecule with diverse therapeutic applications for vaccine development, cellular engineering, and other areas of biomedicine. Alone, however, RNA has little therapeutic potential, being readily degraded by environmental nucleases, and proving ineffective at cellular entry and expression. Delivery vectors are therefore needed to facilitate the protection and transfection of RNAs into cells. For this purpose, organic nanoparticles are most often used. Branched amphiphilic peptide capsules (BAPCs) are a novel class of organic nanoparticles which have previously been shown effective at RNA delivery in various *in vivo* systems with insect and murine models. Previously, BAPC peptides have varied significantly between batches and dependent on the synthesizer, resulting in high variation in experimental BAPC formulation impurities and results. BAPC toxicity has also received little investigation and never been directly compared with major FDA-approved or clinically used nanoparticle formulations such as lipid nanoparticles (LNPs). Here, I outline standardized synthesis, purification, and assembly protocols for branched amphiphilic peptides which compose BAPCs. Furthermore, I investigate potential mechanisms associated with BAPC toxicity in comparison to LNPs and elucidate potential avenues for the improvement of BAPC formulations moving forward. This work will allow for high-fidelity reproduction of BAPCs on any

synthetic-chemistry capable lab bench. Further, this work outlines a comparable level of toxicity for BAPCs when compared to leading lipid alternatives, impressing the potential of this platform as a future clinically-relevant nanoformulation.

Acknowledgments

I would like to thank Dr. Adriana Avila Flores, my advisor, for her guidance and support throughout my time at Auburn. I would also like to extend my sincerest appreciation to the members of my committee, Dr. Alexey Petrov and Dr. Katherine Rush for their support and guidance on various projects. Thank you to Dr. Mohtadin Hashemi and Bruno Henrique Lisenko Ribeiro for their collaboration on several projects as well. My heartfelt thanks go to my senior lab mates Nitish Kunte and Erin McGraw as well for their guidance and support. Last but certainly not least, I am tremendously thankful to my parents, Misti and Rory Wall for their unwavering support, love, patience, and encouragement throughout my life, and to all of my colleagues and friends at Auburn for the same.

Table of Contents

Table of Tables

Table of Figures

Chapter 1: RNA as a Versatile Therapeutic

1.0 RNA in medicine

Diseases stemming from viruses and bacteria as well as genetic disorders are major public health concerns in the US and abroad. Recently, we have begun to understand how these diseases function and elucidate their reliance on gene products. Viruses and bacteria rely on certain proteins and nucleic acids for pathogenicity, and genetic diseases are often deleterious due to deficiencies or abnormalities in proteins or nucleic acids. In modern efforts to combat these issues related to gene products, RNA stands out as a powerful therapeutic.[1]

Ribonucleic acids (RNAs) come in several multi-use forms. Short-interfering (siRNA) are 23-25 bp dsRNA sequences which can induce the degradation or steric inhibition of messenger RNA (mRNA) and silencing of gene products.[2] Inside of cells, siRNA complex with one of four argonaut proteins within humans to form the RNA-induced silencing complex (RISC) which either cleaves mRNA or sterically inhibits translation. Argonaut (ago) proteins 1, 3, and 4 result in steric inhibition, while ago 2 guides nucleolytic cleavage of mRNA dependent on the ago protein (Fig. 1).[2] siRNA therefore has broad applicability to diseases which can be treated via the inhibition of certain gene products.[2]

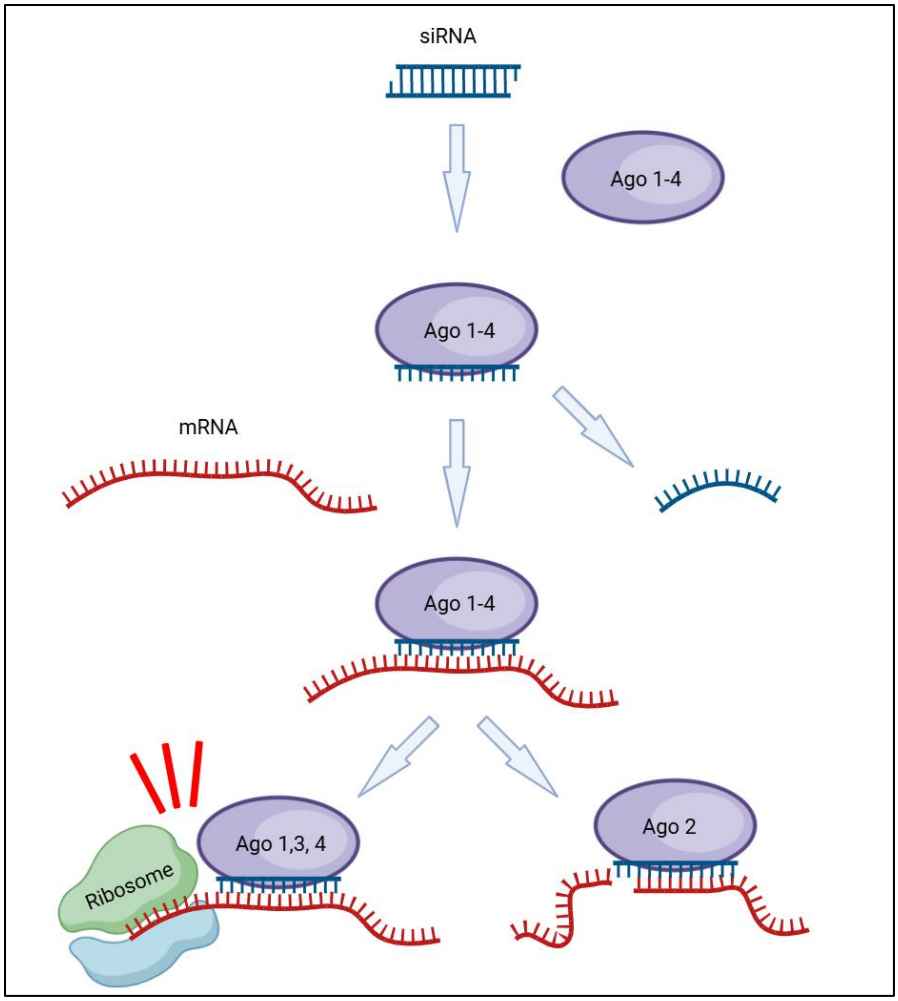

Figure 1: Human siRNA Effector Mechanism. siRNA complex with Ago proteins, where one strand is preferentially selected, and another is shed. Ago-RNA complexes then induce mRNA inhibition via steric hindrance or nucleolytic cleavage.

Some conditions related to gene expression can be treated by siRNAs.[2] Hereditary amyloidogenic transthyretin is caused by the expression of a mutated amyloid protein which builds up and resists degradation in affected patients.[3] ONPATTRO was the first FDA-approved siRNA therapeutic and allows for the translational inhibition of mutated amyloid transcripts, and by extension mutated protein to be reduced.[3] Hypercholesterolemia can be caused by the overexpression of the cholesterol-raising PCSK9 protein in hepatocytes.[4] PCSK9-inhibitor siRNAs can be used to reduce PCSK9 and by extension cholesterol levels.[4]

Certain conditions resultant from mutated gene products can also be alleviated by reducing expression levels of either the mutated protein or tertiary related enzymes.[2] Acute hepatic porphyria is caused by the mutation of one or more genes involved in heme production in the liver leading to the buildup of neurotoxic intermediates.[5] ALAS1 is the primary regulator of heme production, and by lowering ALAS1 levels, the amount of intermediates can be lowered as well.[5] The FDA has approved GIVLAARI for the treatment of acute hepatic porphyria.[5]

Cancers are often caused by the overexpression of certain normal or mutated gene products.[6] Ras genes are involved in the transduction of cell-growth signals.[6] Mutations of such genes can result in dysregulated cell growth and cancerous phenotypes.[6] One such mutation is KRAS-G12D. siRNA targeting transcripts with this mutation are currently being tested at MD-Anderson.[7] Many cancers are hormone-dependent as well. Androgen receptors serve as a source of cell-growth and proliferation signals for prostate and other cancers. A last-resort treatment option involves castration and removal of androgen-producing cells. Some cancers prove to be castration-resistant, however, due to overexpression or mutation of androgen receptors. SXLO1 is being developed as an siRNA targeted against androgen receptors for the treatment of castration-resistant prostate carcinoma.[8]

siRNA have applications as antivirals as well. All viruses must make mRNA and are defined by the route they take to produce it. Viral protein products are necessary for every aspect of virus replication, assembly, escape, entry and uncoating. siRNA can therefore be used to inhibit and degrade important parts of every known virus. JNJ-3989 is an siRNA that can inhibit or degrade all hepatitis B virus transcripts, and has exhibited efficacy in a phase II study.[9] Single stranded RNA virus genomes can be targeted and directly degraded by siRNA. The positive sense RNA

genome of Hepatitis C Virus (HCV) functions as both genetic information and mRNA. siRNAs targeted against this genome have been shown to reduce HCV replication in mouse models.[10]

siRNA have also recently shown potential as antifungal agents. Genes encoding for the RNAi pathway are not encoded in every fungal genome. *Saccharomyces cerevisiae* yeast for example, lacks ago, dicer, and RdRP homologs.[11] Many clinically relevant fungus such as *Candida albicans* however, do contain the necessary genes and proteins to enact RNAi.[12] Various studies have shown the introduction of siRNA and manipulation of RNAi in *Candida* as a viable means of reducing fungal growth and proliferation.[12]

Alternatively, gene expression can be introduced or boosted via treatment with mRNA therapeutics. mRNA are translated to express encoded proteins which can be used to substitute defective or mutated forms of essential genes, or to introduce new proteins. While there are not currently any mRNA protein replacement therapies, several are currently undergoing clinical trials. One such clinical trial involves the delivery of ARC-810, an mRNA encoding ornithine transcarbamylase (OTC) to treat OTC deficiency caused by an X-linked mutation.[13]

New proteins can also be transfected to develop immune responses in patients for vaccination. A recent, FDA-approved example are the Pfizer and Moderna COVID-19 (SARS-CoV-2) vaccines. With COVID-19 vaccines, mRNA is delivered *in vivo* to express a viral protein.[14] Patient immune systems interact with this exogenous protein, resulting in the conferral of varying degrees of immunity to patients against viruses containing the mRNA-encoded protein.[14]

mRNA can also be used to deliver gene-editing technologies to correct aberrant mutations. Recently, the FDA has approved an mRNA-dependent method for sickle cell anemia treatment.[15] Sickle cell anemia is caused by a single point mutation. To cure sickle cell, bone marrow from

afflicted patients is removed and gene-editing proteins encoded by mRNA are introduced *in vitro*.[15] The gene editing proteins are expressed and modify cells to revert a sickle cell point mutation, restoring normal phenotype before reintroduction to patient bones.[15]

1.1 Challenges with RNA-based Therapeutics

RNA is readily degraded by serum nucleases.[16] Furthermore, RNAs are negatively charged and repelled from cellular membranes via electrostatic interactions. If a nucleic acid was to be taken up by a cell, it would likely be done via endocytosis and thus encounter innate host defense mechanisms including inflammatory nucleic acid-binding receptors and degradative enzymes.[16] To be effective, a nucleic acid must be protected from these obstacles and guided within a target cell. Protection and guidance can be performed by a variety of physical, biological, and synthetic methods.

Physical methods involve the permeabilization of cellular membranes, which temporarily allows nucleic acids to pass into them.[17] Membrane permeabilization can be obtained by the application of magnetic, electromagnetic, sonic, physical, and/or electronic energies via magneto oration, photoporation, sonoporation, mechanoporation, or electroporation. Certain chemicals have also been reported capable of increasing membrane permeability. Pelargonidin, derived from strawberries, has been reported to increase membrane permeability and allow for the oral delivery of proteins.[18]

Biological agents include viruses and bacteria. Viral genomes can be modified to various extents to reduce virulence, pathogenicity, and include desirable nucleic acids. Some bacteria can be used to delivery nucleic acids of interest through a process known as bactofection as well. *Salmonella typhimurium* has previously been used as a gene therapy vector against murine

tumors.[19] Intracellular bacteria such as *Salmonella typhimurium* can be loaded with nucleic acids of interest and allowed to infect cells. Upon infection, host cells can kill the bacteria, causing nucleic release, or an antibiotic can be introduced for the same result.[19] Biological methods may not be preferred, however as they can readily activate innate immune defenses which may result in inflammation as well as suboptimal RNA expression and poor therapeutic outcomes.

1.2 Nanoparticle Delivery Vectors

Synthetic transfection agents include a diverse number of drugs designed to combat and solve issues of nuclease protection, cellular entry, immune evasion, and endosomal escape. Primary subcategories of transfection agents include inorganic and organic nanoparticles (Fig. 2). Inorganic nanoparticles are made of metals or composites. While less frequently used for nucleic acid delivery, inorganic nanoparticles can be used to encase, bind, and deliver nucleic acids.[20] Organic nanoparticles are often further subcategorized into polymeric and lipid-based technologies. Polymeric nanoparticles involve long, often positively charged polymers made of organic materials. The polymers bind negatively charged nucleic acids and protect them from degradation and immune detection. Positive charges help to initiate cellular entry via interactions with membrane lipids and proteins. Lipid nanoparticles differ from polymeric nanoparticles in their structure. While polymeric nanoparticles involve long, polymeric chains, lipid nanoparticles are composed of monomer lipids. Like polymeric nanoparticles, lipid nanoparticles include positively charged species which function to bind nucleic acids and induce cellular uptake.

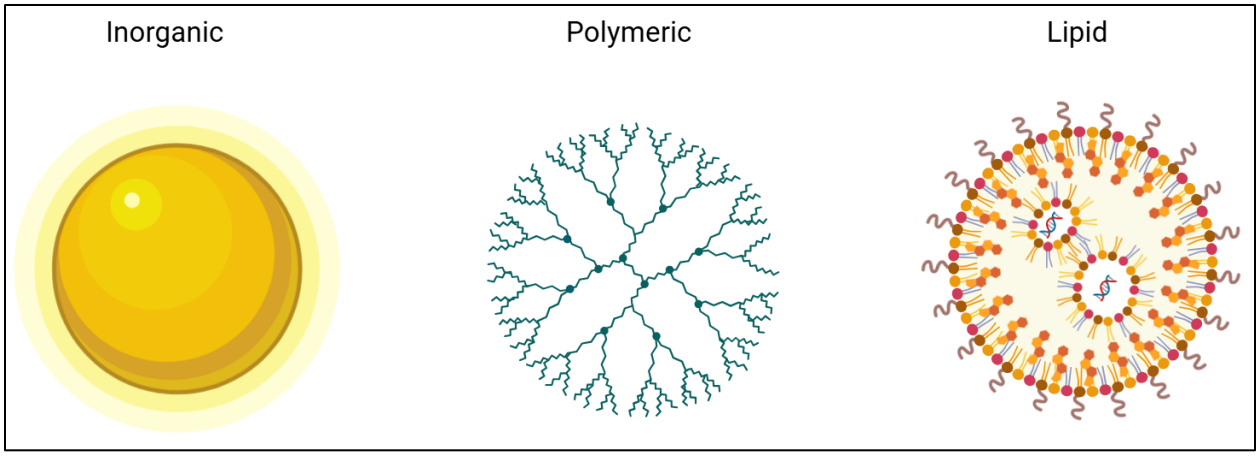

Figure 2: Nanoparticle Classes. Inorganic nanoparticles and organic polymeric and lipid-based technologies.

The most studied and used delivery vectors to date are lipid nanoparticles (LNPs).[16,21] The Moderna and Pfizer COVID-19 vaccines were both delivered with LNP formulations, and LNPs are used for other clinical applications as well. LNPs are small 30-100 nm nanoparticles composed of lipid monomers and other additives.[22] Nucleic acid condensation and encapsulation are mediated by ionizable or positively charged amines present on some lipid components. Microfluidics are implemented to ensure uniform nanoparticle size distributions during formation and maximize RNA encapsulation within the nanoparticles.[16] When encapsulated, RNAs are protected from serum degradation.[16] Nanoparticle stability varies depending on formulation, and steric inhibitors such as polyethylene glycol (PEG) are often used to inhibit LNP-LNP interactions. Optimal size for the reduction of cytotoxicity and increased cellular uptake has been shown to be around 30 nm depending on formulation.[22] Exact metabolic pathways for the digestion of LNP lipids varies and is not completely understood as many of the lipids used in LNPs are of synthetic and unnatural origin.

Synthetic transfection reagents are often internalized via endocytosis. Once in an endosome, a transfection reagent must destabilize it to allow for release of its complexed drug.[23] Failure to escape an endosome will result in endosomal maturation into a lysosome, wherein RNAs will be

degraded and rendered useless. Escape can be performed through a variety of mechanisms as seen in Figure 3. Membrane fusion and destabilization can result from the presence of fusion proteins or charged residues present in the delivery nanoformulation (Fig. 3a, d). Osmotic rupture, also known as the proton sponge effect, results from the nanoformulation buffering capacity. As an endosome attempts to reduce its pH and evolve into a lysosome, buffers can prevent this, resulting in an over-influx of ions and water molecules and endosomal bursting (Fig. 3b). Particle swelling can result from various engineered aspects of a nanoformulation such as pH dependent conformational changes (Fig. 3c).

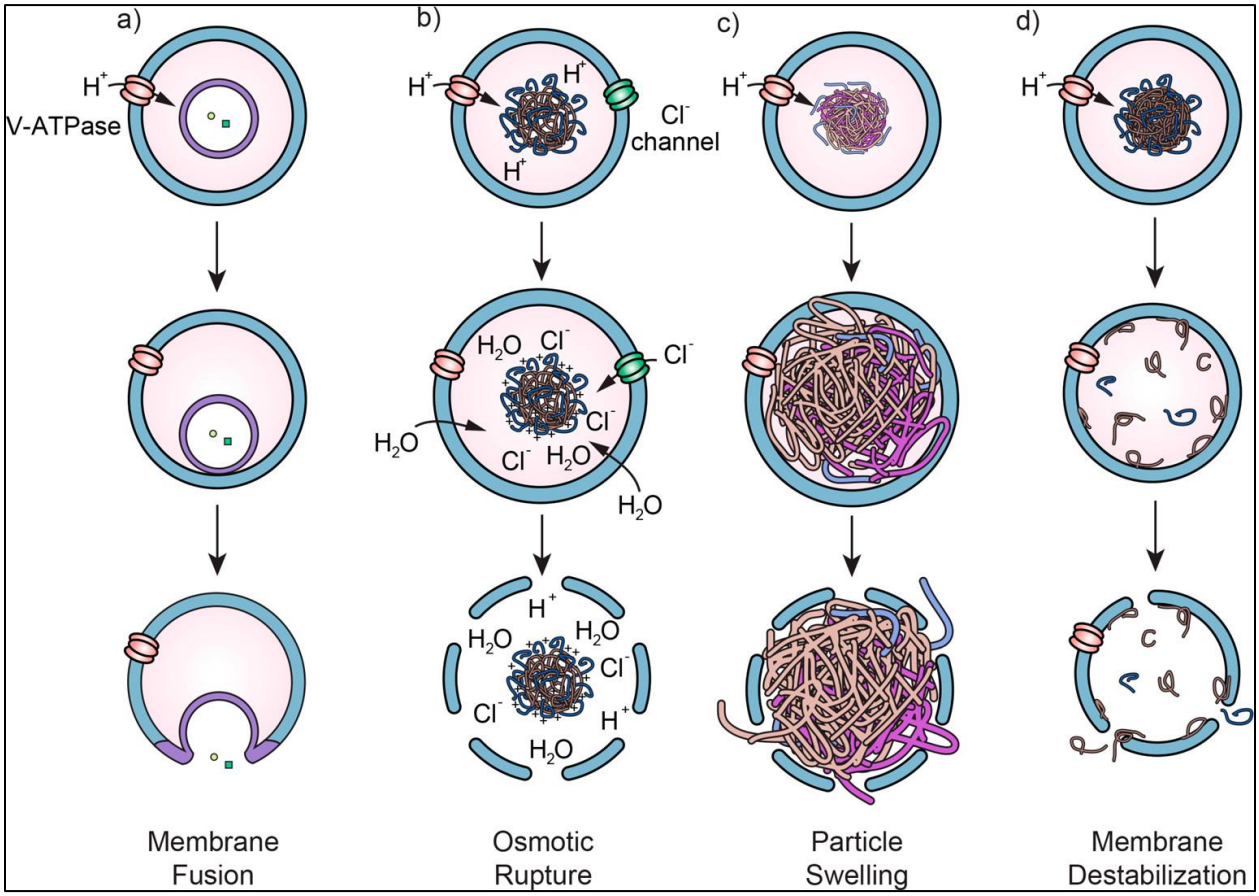

Figure 3: Mechanisms of endosomal escape. (a) Membrane fusion between a nanoparticle and an endosomal membrane. (b) The proton sponge mechanism whereby nanoparticle buffering capacity increases the influx of chloride counterions during endo/lysosome maturation and lyses the endo/lysosome due to increased osmotic pressure. (c) Endosomal rupture facilitated through mechanical strain induced by a pH responsive nanoparticle. (d) pH responsive nanoparticles destabilize an endosomal membrane via direct chemical interactions.[23]

1.3 Branched Amphiphilic Peptide Capsules

Branched Amphiphilic Peptide Capsules (BAPCs) were first developed by Dr. Adriana Avila-Flores et. al at Kansas State in 2010.[24] Originally investigating the adhesive properties of hydrophobic peptide sequences in search of glue, Flores et. al discovered two sequences IVILF and IISGIVILF which originally aggregated as nanofibers when coupled with lysine residues to form $K[IVILF]_2$ and $K[IISGIVILF]_2$. The FLIVIGSII sequence itself originated from the membrane-bound section of a heart tissue calcium ion channel protein.[24] Inclusion of additional lysine groups and the bifurcation of hydrophobic tail segments to yield $KKKKK[IVILF]_2$ (h5) and $KKKKK[IISGIVILF]_2$ (h9) resulted in the formation of charged, spherical nanoparticles capable of solute encapsulation (Fig. 4).[24,25]

Upon suspension in room temperature water, BAPC peptides were found to rapidly form fusogenic particles, and increase in size from the nanometer to micron range.[25] Out of multiple attempts to limit and homogenize BAPC size, it was found that refrigeration after a period of room temperature BAPC formation resulted in thermostable nanoparticles.[26] The extent of formation times directly correlated to nanoparticle size and homogeneity.[26]

Investigation found BAPCs to feature a peptide bilayer, peptide charged lysine residues exposed to solvent interfaces, where h9 peptides likely favored the outside bilayer and h5 peptides composed the external surface of the nanoparticles (Fig. 4).[27] The hydrophobic residue tail-sections were observed to form beta-sheet-like characteristics, and phenylalanine residue side chains were observed to engage in pi-stacking.[27]

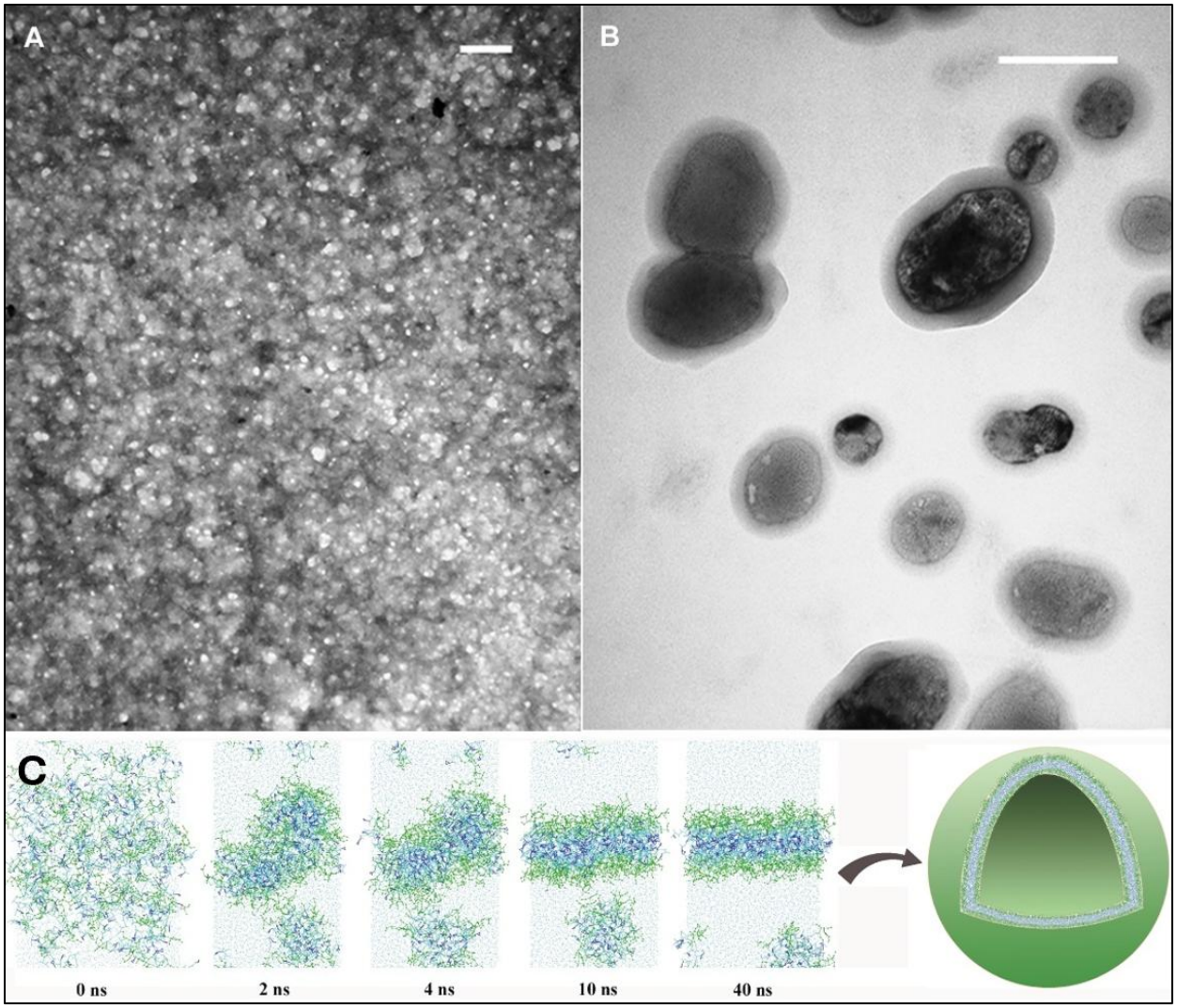

Figure 4: ***Biophysical Characteristics of BAPCs.*** TEM images of (A) a concentrated and (B) a diluted sample of the peptide mixture, stained with 5% phosphotungstic acid and Osmium tetroxide (OsO4) vapors, respectively (200 nm scale bar).. (C) A coarse-grained simulation of h5 bilayer self-assembly.[24]

BAPCs were found capable of solute and drug encapsulation and experimented with as chemotherapeutic delivery vectors.[28,29] Positively charged lysine residues further allow for the complexation and condensation of nucleic acids such as DNA.[30] While hydrophobic chemotherapeutic and dyes are relatively easily encapsulated, complexation with negatively charged molecules during BAPC formation was found to result in peptide aggregation and formation of large complexes. Thus, preformation of BAPCs and subsequent complexation was found to be effective at condensing negatively charged DNA molecules. BAPC-DNA complexes

formed in this manner were found capable of transfection both *in vitro* and *in vivo* with mammalian cells and murine models.[31] BAPCs are made of natural peptides and do not require PEGylation for thermostability, thus they present great potential as a biocompatible, synthetic transfection vector for the future.

1.4 BAPC-RNA Interactions

When complexing BAPCs and RNA, BAPCs are first preformed in water or buffer such as 50 mM calcium chloride. After formation, BAPCs are mixed with RNA to form BAPC-RNA clusters (Fig. 5).[32] Negatively charged nucleic acids will adsorb to the positively charged surface of BAPCs, acting as glue to attract other BAPCs. Because mixing is performed spontaneously and at random, a heterogenous mixture of BAPC-mRNA clusters is formed.[32] BAPCs used for cluster formation are often heterogeneously sized before combination with RNA as well. These variably sized clusters (50-500 nm) are then ready to be used for delivery applications.[32]

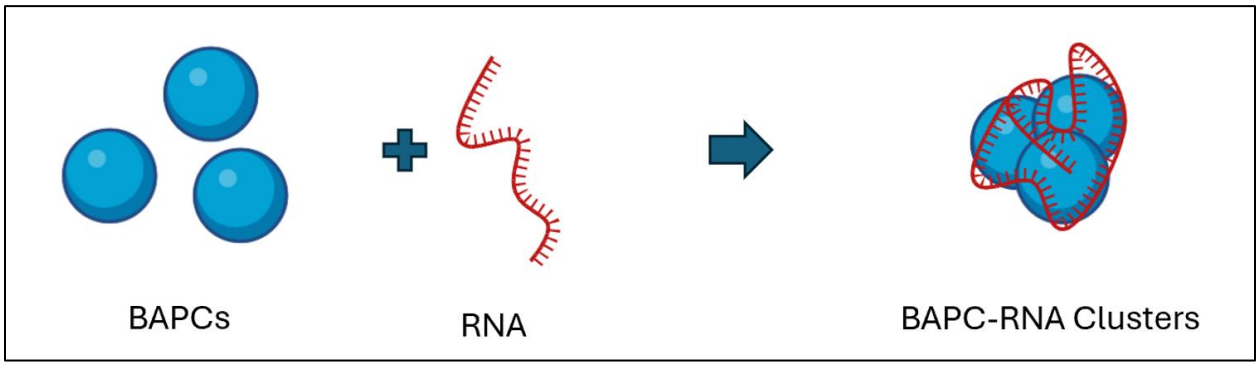

Figure 5: BAPC-RNA Complexation Mechanism. Proposed mechanism through which BAPCs and RNA interact to form large, multi-BAPC/RNA clusters.

BAPC-RNA cluster biodistribution and cellular uptake have been studied *in vivo* and *in vitro*.[32] *In vitro*, BAPCs and BAPC-RNA clusters were found to be taken up by cells largely via clathrin-mediated endocytosis and micropinocytosis.[33] BAPCs and BAPC-mRNA complexes were also found capable of transcytosis across isolated adult *Popillia japonica* gut epithelium.[33] When fed

orally to Tribolium larvae, fluorescent BAPC-dsRNA clusters were found intact after passing through larvae midguts.[34] Furthermore, BAPC-dsRNA clusters targeted against Tribolium dsVermillion gene and fed orally to larvae were found capable of silencing ocular dsVermillion gene expression.[34]

After cellular entry, RNA is hypothesized to separate from BAPCs via displacement by negatively charged molecules present in the cytoplasm such as heparin, a negatively charged polysaccharide present in human cells.[35] Treatment of BAPC-mRNA clusters with concentrations of heparin showed rapid displacement of mRNA.[35] Furthermore, the total displacement of RNA was found to increase with increasing heparin concentrations.[35] After displacement, the fate of BAPC peptides is unknown. Being composed of natural amino acids, BAPCs may be biocompatible and readily metabolized *in vivo* or *in vitro*, however; BAPC peptides have proven resistant to the actions of SDS, urea, and trypsin.[24]

1.5 Research Goals

The aim of this thesis is twofold: 1) to clearly outline and describe synthesis, purification, and assembly procedures for branched amphiphilic peptides and 2) to characterize and investigate *in vitro* transfection and toxicity with BAPC-RNA complexes using purified peptides. Until now, detailed methods for synthesis as well as quality control have not been published. This has made reproducing BAPCs de novo an arduous task. The publication of detailed methods will facilitate ease of synthesis and use among varied labs and ensure reproducibility and quality of results among researchers. Additionally, while BAPCs constructed of purified peptides have been used for several *in vivo* RNA delivery publications, BAPC-mediated RNA delivery remains relatively unexplored *in vitro*. Cellular toxicity of BAPC-RNA complexes also remains an area of interest. This thesis will explore several cytotoxic mechanisms with purified peptides to outline potential

sources of toxicity with importance for both current and future applications as well as insights for how future BAPC sequence modifications might be constructed to minimize toxicity.

Chapter 2: Synthesis and Nanoassembly of Branched Amphiphilic Peptides

2.0 Introduction

Despite the fact that BAPCs have been used for more than 10 years and in several research groups, not much effort have been made on improving purity during the synthesis. A detailed methods article on the synthesis is not currently available and has never been published. While synthesis protocols for peptides are readily available, branched amphiphilic peptide synthesis, specifically with regard to downstream BAPC assembly applications, involves several unique reactions and important quality control steps. Peptides of variable purity have been used in our lab for experimentation (Fig. 6).

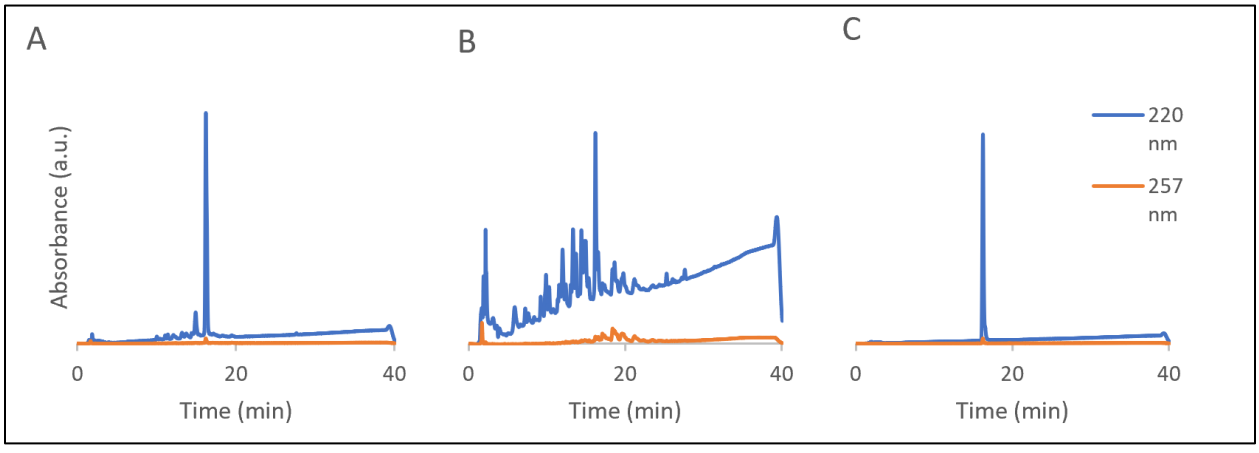

Figure 6: Batch Variability of Branched Amphiphilic Peptides. Chromatograms of different h5 peptide batches in Flores Lab, synthesized in (A) 2015 and (B) 2022 compared to (C) pure h5 peptide.

BAPs are constructed via solid phase peptide synthesis; whereby individual amino acids are added via a repeated set of reactions to a solid-phase support. Upon completion, peptides are

cleaved from their supports and purified before being aliquoted for experimentation. Inefficiencies in reaction steps result in the production of varying impurities which can have major ramifications for experimentation with BAPCs.

BAPs are constructed C to N terminal (Fig. 7). Carboxyl groups of N-terminally protected, free amino acids are activated and used as electrophiles to react with free amino groups of resin-bound, expanding peptide chains. In our lab, and most others, fluorenylmethyloxycarbonyl (FMOC) is used as the primary amine protecting group. FMOC is removed via reaction with piperidine in Dimethylformamide (DMF) at room temperature to form a soluble piperidine adduct, compatible with wash solvents. Additionally, FMOC is a strong UV-absorber, and allows for various quantitative assays to be performed during reaction.

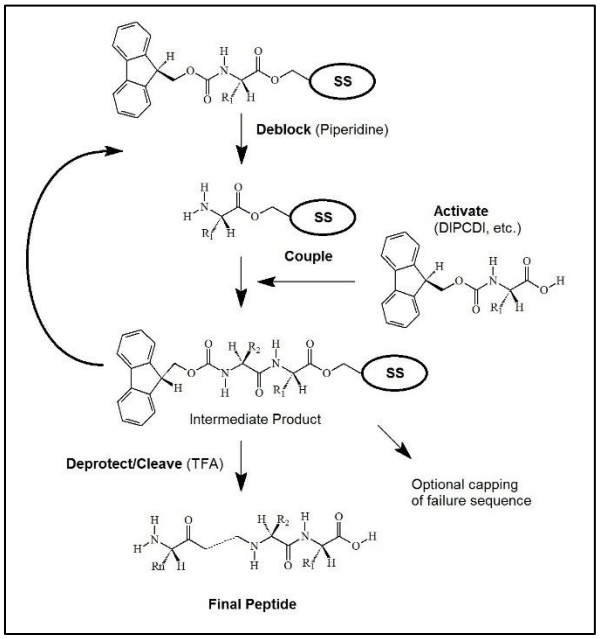

Figure 7: Solid Phase Peptide Synthesis reaction schematic. Peptides are elongated one amino acid at a time from a solid-phase resin via a repeated series of coupling steps.[36]

As a reaction scheme, N-terminal FMOC groups are removed with piperidine. Amino acids to be coupled are then activated with either hexafluorophosphate benzotriazole tetramethyl uronium (HBTU) or 1-hydroxy-7-azabenzotriazole (HOAt) in the presence of either

diisopropylethylamine (DIPEA) or N,N'-diisopropylcarbodiimide (DIC). Activated amino acids are coupled with the free aminos of growing peptides, and the cycle is repeated until a desired sequence is produced. Coupling times may range from 15 minutes to over 16 hours, and in our experience, longer coupling times only benefit reaction yields. Coupling times and by extension yields may be optimized and tested via the ninhydrin test.

Peptide branching is achieved via the use of an FMOC-FMOC-lysine or other selectively-deprotectable lysine side chain such as DDE. After coupling to an existing chain, both the backbone and side chain amines are deprotected, allowing subsequent coupling reactions to take place at both sites, resulting in a branched peptide.

Crude peptides obtained from synthesis contain large percentages of impurities. Purities as measured by fractional 220 nm absorbance of peptides synthesized in our lab often range from 30-70%. These impurities can involve peptides as well as linker decomposition products and other chemical residues generated during cleavage. BAPC formation and usage inclusive of these impurities could result in results wrongfully being attributed to a target synthesis product and so should be removed. Additionally, BAPCs are prepared, as will be discussed in section 3.3, using UV absorbance. Impurities, especially aromatics, will greatly affect absorbance readings, and can lead to inaccurate BAPC concentrations downstream.

Peptide purification and analysis can be routinely performed via high performance liquid chromatography, whereby peptides are dissolved in a mobile phase and separated based on interactions with a column-packed stationary phase. Our lab uses reverse-phase, C-18 columns in tandem with acidified water/acetonitrile mobile phases to perform both analytical and preparative operations for all of our peptides. Acidification of mobile phases ensures protonation of stationary phase silenol groups and analytes, providing for sharp elution peaks.[37] Acids also

act as counterions for analytes and have significant effects on their elution profiles.[37] In our lab, we have found variance between trifluoroacetic acid (TFA) and significantly less hydrophobic formic acid to be sufficient for the analysis and purification of all peptides on C-18 columns.

In this chapter, I will outline standardized production protocols for BAPs, beginning with chemical synthesis and ending with HPLC purification and nanoparticle assembly, and impress the significance of maintaining batch purity for both published and unpublished experimentation.

2.1 Materials and Methods

2.1.1 Materials

Acetonitrile (VWR, USA), 2,2,2-Trifluoethanol (VWR,USA), Fmoc-Amino acids (Ambeed, USA), Fmoc-lys-dde (Ambeed, USA), Trifluoracetic Acid (VWR, USA), Zorbax C-18 Column (300 Å, 5 µm, 9.4 mm x 150 mm) (Agilent, USA), Xterra C-18 Column (100 Å, 5 µm, 4.6 mm x 150 mm) (Waters, USA), 1,3-Dimethoxybenzene (VWR, USA), Triisopropylsilane (VWR, USA), N,N'-Diisopropylcarbodiimide (VWR, USA), HBTU (Ambeed, USA), HoAT (VWR, USA), SPPS reaction cartridges and caps (RESTEK, USA), Ultra-Pure Agarose (VWR, USA), 10X MOPS buffer (VWR, USA) SDS-free gel loading buffer (New England Biolabs, USA).

2.1.2 Ninhydrin Test

REAGENTS:

Reagent A (If don't have KCN, just use pyridine):

1. Dissolve 16.5 mg of KCN in 25 mL of distilled water.
2. Dilute 1.0 mL of above solution with 49 mL of pyridine (freshly distilled from ninhydrin).

Reagent B:

1. Dissolve 1.0 g of ninhydrin in 20 mL of n-butanol.

Reagent C:

1. Dissolve 40 g of phenol in 20 mL of n-butanol.

PROCEDURE

1. Take 10-15 beads of resin in a test tube and label it S.

2. Take tube S and another empty tube designated R (reference)
3. To each tube add:

   2 to 3 drops of Reagent A
   2 to 3 drops of Reagent B
   2 to 3 drops of Reagent C

4. Heat both the tubes at 110°C for 5 minutes.
5. Compare the color with reference.

Result	***Meaning***
Colorless or faint blue color	complete coupling, proceed with synthesis
Dark blue solution but beads are colorless	nearly complete coupling, extend coupling or cap unreacted chains
Solution is light blue but beads are dark blue	coupling incomplete, recouple
Solution is intense blue and all beads are blue	failed coupling, check amino acid, reagents, then recouple

2.1.3 FMOC-SPPS

Swelling the Resin

2. Insert the white frit into the synthesis cartridge and cap the bottom.
3. Add 500 mg of rink resin a 10 mL synthesis cartridge.
4. Fill the cartridge about 3/4 of the way with DCM. (DO NOT CAP THE TOP!!)
5. Allow the resin to swell in the fume hood for at least 2 hours.
6. Drain the synthesis cartridge using a vacuum flask.

Rinsing

1. Rinse the resin with DCM and drain.
2. Rinse the resin with MeOH and drain.
3. Rinse the resin with DMF and drain.
4. Repeat steps 1-3 two additional times.
   Note: If you'd like to stop and store the peptide, then after the rinsing protocol, rinse with DCM, drain, then store. Make sure to leave an opening for DCM to evaporate out of as it is volatile.

Fmoc Deprotection

1. To the swollen resin, fill the synthesis cartridge with 1 ml/100 mg of 20% piperidine in DMF.
2. Cap the synthesis cartridge.
3. Put the synthesis cartridge on the wrist action shaker for 15 minutes (1 hour for first deprotection).

4. Remove from the shaker, drain the solvent and follow the rinsing protocol.

First Coupling

1. In a glass scintillation vial combine 6 equivalents of the amino acid to be coupled, 6 equivalents of DIC, and 6 equivalents of HOAt. Equivalents are based on the millimoles of resin used. For this case, 500 mg of resin is 0.25 mmol because rink resin's molar mass is 0.50 mmol/g. Thus 1 equivalent to 500 mg of resin is 0.25 mmol.
2. Add DMF to the scintillation vial and mix as needed until the reagents are dissolved.
3. Add the contents of the scintillation vial to the resin. The solution will likely be a yellow color.
4. Cap the synthesis cartridge and put it on the wrist action shaker for 4 hours.
5. Remove from the shaker, drain the solvent, and follow the rinsing protocol.

Capping

1. Drain the reaction cartridge and follow the rinsing protocol.
2. Perform a ninhydrin test to see if capping is needed.
3. Prepare the capping solution by combining acetic anhydride and pyridine in a 3:2 ratio of acetic anhydride:pyridine. Make this fresh each time. Crudely, by using a Pasteur pipette, combine 3 "squirts" of acetic anhydride with 2 "squirts" of pyridine in a scintillation vial.
4. Dump the capping solution on the resin and rock for 30 min at room Temperature.
5. Perform another ninhydrin test and repeat as necessary until negative.

Quantification of Loading

1. Drain the reaction cartridge and follow the rinsing protocol.
2. Dry out the resin over vacuum for a minute.
3. Measure 1 mg of resin from the cartridge and put in a glass scintillation vial.
4. Add 20% piperidine in DMF and deprotect.
5. Measure sample UV absorbance at 301nm, calculate amount of amino acid loaded for future calculations.

Subsequent Couplings

1. Follow the Fmoc Deprotection protocol.
2. In a glass scintillation vial combine 4 equivalents of the amino acid to be couples, 4 equivalents of HBTU, and 4 equivalents of DIPEA.
3. Add 8 mL DMF (little over ¾ full) to the scintillation vial and mix as needed until the reagents are dissolved.
4. Let rest for ~15 minutes, then add the contents of the scintillation vial to the resin.
5. Cap the synthesis cartridge and put it on the wrist action shaker for 15 minutes – 2 hours.
6. Remove from the shaker, drain the solvent, and follow the rinsing protocol.

Cleaving from the Rink Amide Resin

1. After coupling the last amino acid, follow the Fmoc Deprotection protocol once more.
2. Cap with acetic anhydride/pyridine.
3. After rinsing the resin, rinse it with DCM, drain, and allow it to dry for about 15 minutes on the vacuum (until sandy).
4. Add 20 mL/g of an 9.25:0.5:0.25 TFA:DMB:TIPS to the resin.
5. Seal and place on the wrist action shaker for 3 hours.

6. The peptide should now be in solution. Allow the solution to dry under air. The crude product will be left over after drying.

Cleaving from the Chlorotrityl Resin

1. 2% TFA/DCM for 30 minutes (20 mL/g)

Ether Precipitation

1. Chill diethyl ether over ice (or dry ice, if available) for 30-60 minutes while the crude product is air drying.
2. Filter the solution into a 50 mL tube.
3. Add 10 mL of ice-cold ether per mL TFA/peptide solution to the 50 mL tube.
4. Incubate in an ice bath for 15-20 minutes as the peptide precipitates.
5. Pellet the precipitated peptide by centrifugation. The pellet is your peptide.
6. Decant the ether supernatant into another vessel. Do not discard until you have confirmed that your peptide is in the pellet.
7. Transfer each pellet to a round bottom flask by adding acetonitrile to each pellet.
8. Dry the pellet.

2.1.4 Analytical HPLC

Crude and purified peptide products were analyzed for impurities via reverse-phase high pressure liquid chromatography using an Xterra C-18 column (100 Å, 5 µm, 4.6 mm x 150 mm). Masses of peptides ranging from 0.1-1 µg were dissolved in 200 µL of 20% ACN/H_2O with 0.76% v/v TFA. Species were then analyzed via a gradient elution, increasing from 20-80% ACN/TFA over a period of 30 minutes at 1 mL/min. UV absorbances at 220 nm and 280 nm were recorded corresponding to the presence of peptide bonds and aromatic species accordingly. Purified peptides were analyzed at 220 nm and 257 nm to determine spectral purity coefficients and peptide extinction coefficients for subsequent aliquoting.

2.1.5 Preparative HPLC

10-40 mg amounts of crude peptides were dissolved in 0.5-1.5 mL of 20% ACN/TFA in H_2O/TFA. To expedite peptide dissolution, peptides were first added to 80% ACN/TFA in H_2O/TFA and then diluted to 20% with H_2O/TFA. These solutions were applied to a Zorbax C18

semipreparative RP-HPLC column (300 Å, 5 µm, 9.4 mm x 250 mm). Following, peptides were purified via a 2 mL/min room temperature, AB gradient elution, where eluent A is 0.076% aqueous TFA, and eluent B is 0.076% TFA in ACN. To design the gradient method, establish the percentage "X" of ACN required to elute the peptide analytically using the same mobile phases as will be used here. Begin a run by increasing ACN concentration from 20% ACN to a value 12% below X over 30 minutes. Once an ACN concentration 12% below X is reached, begin a gradient increasing ACN concentration by 0.1% per minute for 150 minutes. Samples should elute during the 0.1% gradient. Fractions should be collected during the 150 minute gradient and can be further optimized for additional purifications.

UV absorbances at 220 and 280 nm should be recorded during elution. Substantial absorbances recorded at 280 nm can be used to identify impurities and linker residues attached to h5, h9, and other peptides which do not include residues that absorb at this wavelength. Furthermore, due to the relative chemical properties of peptides and adduct-conjugated peptides, 280 nm absorbance peaks can be used as approximations of individual crude product elution times to optimize fractionation.

Fractions can be directly checked for the presence of target peptides via analytical HPLC or mass spectrometry; they can also be lyophilized and then checked. Fractions containing pure peptides or minimal impurities should be pooled.

For very hydrophobic peptides such as h9, 0.0377% v/v formic acid was substituted in mobile phases for TFA. Elution peaks will often change with mass load and varying crude yields (variable concentrations of crude species). To account for varying elution peaks, fractions should

be collected around optimized elution peaks (±10 minutes) when changing mass loads or between crude batches.

2.1.6 Atomic Force Microscopy

Following incubation at 4℃ for one-hour, fresh 100μM BAPC nanoparticle stocks with and without mRNA were used as the 0-hour sample for AFM imaging. The stock solutions were then incubated for an additional 3 weeks, at 4℃. Aliquots were removed from the stock solutions at a weekly interval and used for AFM imaging. For AFM imaging under ambient conditions the aliquot was deposited on freshly cleaved mica. Briefly, 50 μl of solution was deposited on the mica surface, incubated for 2 minutes, rinsed with deionized water, dried with a gentle stream of air, and stored under vacuum until imaged. Imaging was performed on a NanoWizard ULTRA Speed 3 (Bruker Nano GmbH, Berlin, Germany) system using Multi75GD-G or Tap150Al-G (BudgetSensors, Sofia, Bulgaria) AFM probes with nominal spring constants of 3 or 5 N/m, respectively. AFM imaging was conducted in Quantitative Imaging (QI) Advanced mode using 15 nN force, yielding both topographic and nanomechanimal characterization. A typical AFM image scanned 2x2 μm area with 512 samples/line. Analysis was performed using the Bruker JPK data analysis software and Gwyddion (https://www.gwyddion.net).

2.1.7 Gel Retardation

BAPCs were preformed and then complexed with 1 ug of mRNA at various N:P ratios, “N:P ratio” relating the amount of positively charged nitrogen species in a given amount of BAPCs to the amount of negatively charged phosphates in an amount of RNA. After 10 min of incubation at room temperature, all samples were mixed at 1:6 ratios with gel loading buffer. Then, samples were loaded on a 2% agarose gel containing 1X MOPS- buffer and 1X Syber Green II and

electrophoresed at 50 V for 1 hour on ice. 1 µg of only mRNA was included as a control. After electrophoresis, the mRNA bands were visualized using ImageQuant LAS 4000 (GE Healthcare, Pittsburgh, PA, USA).

2.1.8 Aliquoting BAPCs

To produce an aliquot of BAPCs, extinction coefficients of uniquely absorbing residues such as phenylalanine, which are present on a purified peptide, are summed at a wavelength of interest to approximate a peptide's extinction coefficient. Purified peptides are then analyzed via analytical HPLC to determine the spectral purity of the peptide in a given sample at the desired extinction coefficient's wavelength. Purified species often contain minor impurities which can significantly affect UV absorbance, and it is imperative that these impurities are quantified before aliquoting. Peptide UV absorbance is then measured via spectrophotometric absorbance of peptides dissolved in TFE. TFE is used to prevent capsule formation.[24] Extinction coefficients of peptide bonds can also be approximated using https://nickanthis.com/tools/a205.html. Concentrations can then be determined via Beer-Lambert's law, and peptides can be aliquoted. Following aliquoting, peptides must be lyophilized. Peptides are dissolved into a 1:1:1 solution of ACN:TFE:H_2O, frozen with liquid nitrogen, and then lyophilized via centrifugal evaporation.

2.2 Results and Discussion

2.2.1 Coupling Times

Previously, coupling times were limited to 5-minute intervals. It has been reported elsewhere that while 5-minute coupling times may prove sufficient for early residues, extended chains often require longer reaction times to achieve high yields.[38] To optimize coupling times, I quantified free, unreacted amines via the ninhydrin test. Coupling times were extended until a negative

ninhydrin test result was obtained. Optimized coupling times are displayed in Table 1 and feature lengths of time significantly increased from our lab's original 5-minute intervals.

Residue	K	K	K	K	K	I	I	S	G	I	V	I	L	F
Coupling Time (minutes)	-	15	15	15	15	15	15	30	15	20	25	45	45	60

Table 1: Optimized SPPS coupling times. Coupling times of individual h9 residues optimized via ninhydrin testing. Peptides were coupled sequentially from left to right.

As seen in Figure 8, extension of coupling times reduces the number of individual species of impurities in crude products and the yield of our target peptide. Crude product yields as estimated by 220 nm absorbance estimate an increase of yield from less than 1% to 22.84% following coupling time extensions.

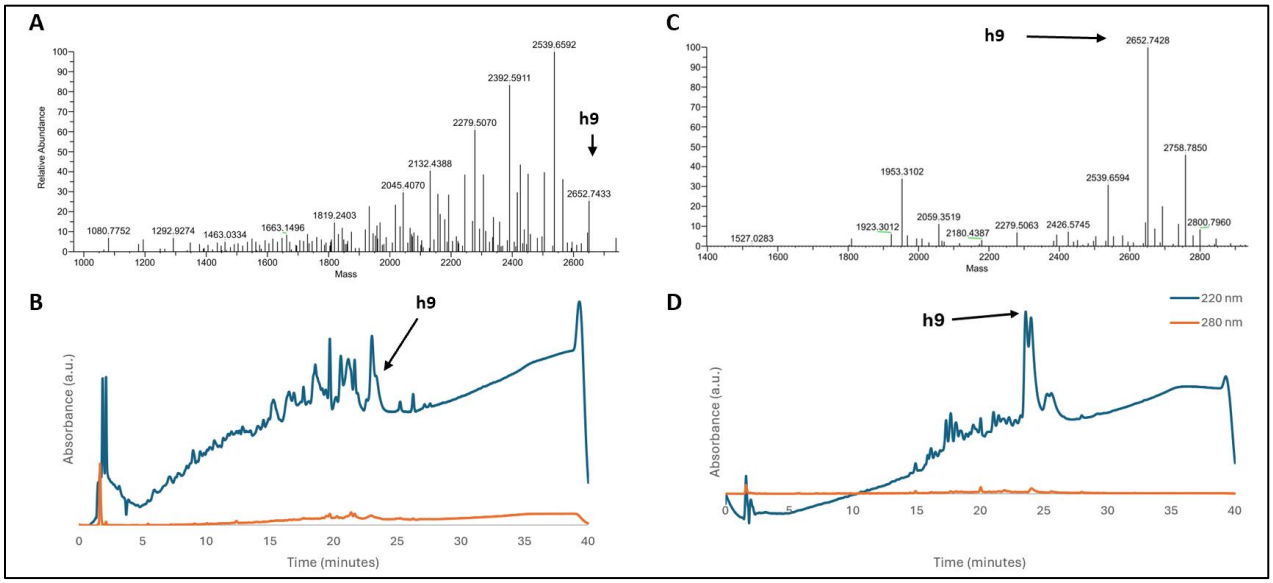

Figure 8: Effect of coupling time extensions on crude products. (A) Electron spray mass spectrometry and (B) HPLC data analysis of crude products made without coupling time extensions. (C) Electron spray mass spectrometry and (D) HPLC data analysis of crude products made with coupling time extension.

2.2.2 Benzyl-Adduct Prevention

Mass spectrometry data from crude products revealed the presence of several proposed complete and incomplete peptide impurities containing a +106 Da residue (Fig. 9A, B). This residue has previously been identified by Stathopoulos et al. as likely attributable to a benzyl-adduct attached at peptidyl C-terminus of peptides synthesized on Rink-amide resins.[39] Stathopoulos et al. reported the inclusion of dimethoxybenzene (DMB) at low concentration in peptide cleavage cocktails as preventing adduct formation.[39] Utilizing a cleavage cocktail containing 92.5:0.5:0.25 TFA:DMB:TIPS (as reported by Stathopoulos et al), I was able to prevent adduct formation and increase crude yields from 22.84% to 35.68% (Fig. 9C, D).

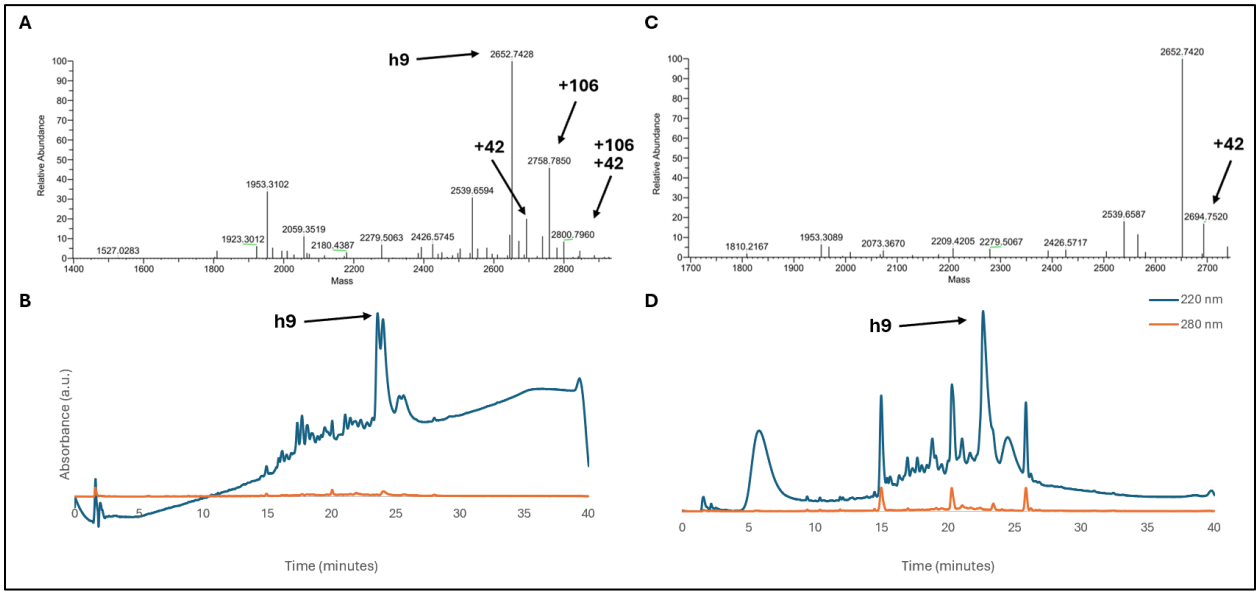

Figure 9: Benzyl-adduct impurity. (A) Mass spectrum and (B) HPLC chromatogram of crude products yielded before the inclusion of 1,3-DMB to cleavage cocktail. (C) Mass spectrum and (D) HPLC chromatogram of crude products yielded after the addition of 1,3-DMB to cleavage cocktail

2.2.3 Fmoc-Serine Protection

The presence of a +42 group was observed in mass spectrometry data of h9 peptides as well (Fig. 9A, B) and observed to account for approximately 10% of crude product yield. Previously, our group had used unprotected FMOC-serine residues for coupling. I hypothesized that this group may react with acetic anhydride during an acetylation step to result in a 42 Da impurity (Fig. 10).

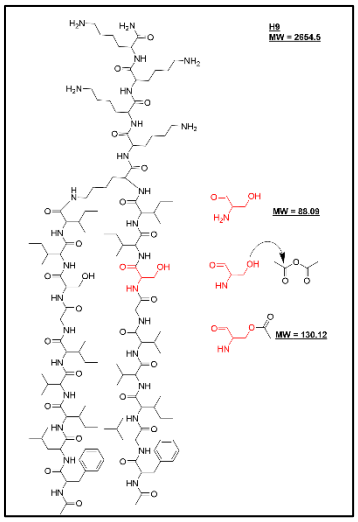

Figure 10: Proposed Mechanism for +42 da impurity. Unprotected serine residues are acetylated via reaction with acetic anhydride, resulting in a +42 da crude product.

Protection of FMOC-serine side chains during synthesis with tert-butyl groups resulted in the complete inhibition of +42 Da species in crude products as seen in Figure 11.

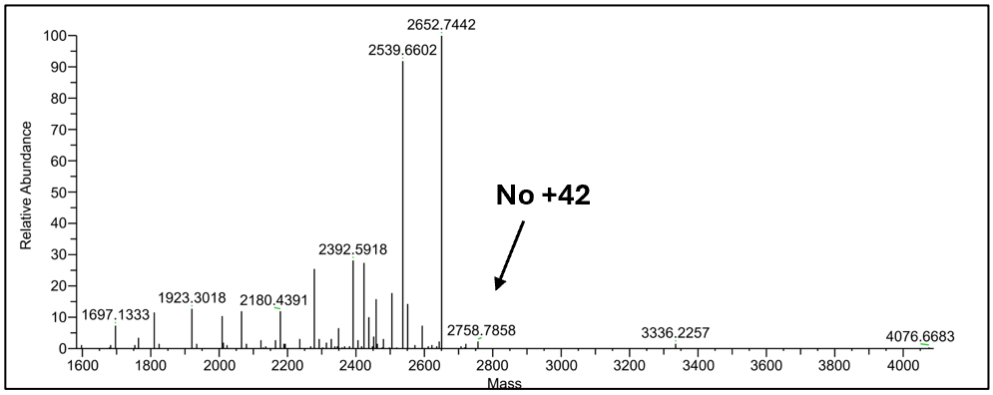

Figure 11: Inhibition of +42 da impurity. Mass Spectrum of crude products resultant from the protection of fmpc-serine side chains with tert-butyl groups.

2.2.4 Preparative Peptide Purification

Preparative purifications of milligram amounts of pure peptides were obtained via high-pressure liquid chromatography using a 9.4mm x 250 mm C-18 column. During scale up from analytical to preparative chromatography, there are several important factors which affect elution profiles including mobile phase velocity.[40] For the analytical column, a linear mobile phase velocity of 60 mm/min was achieved across a 150 mm, 4.6 mm diameter, 5 um, 100 A C-18 column. Our preparative column contains 5um particles with 300 Å pores but measures 9.4 mm diameter and 250 mm length. The Shimadzu HPLC which I used has an upper pressure limit of 3600 psi and the pressure required to obtain the analytical solvent velocity across our prep column would result in pressures greater than 3600 psi and was thus impossible to obtain. As a result, separation of more hydrophobic h9 peptides with TFA-containing mobile phases on prep columns showed skewed elution profiles (Fig. 12A). In comparison to h9, the more hydrophilic h5 peptide was readily purified with TFA mobile phases (Fig. 12B).

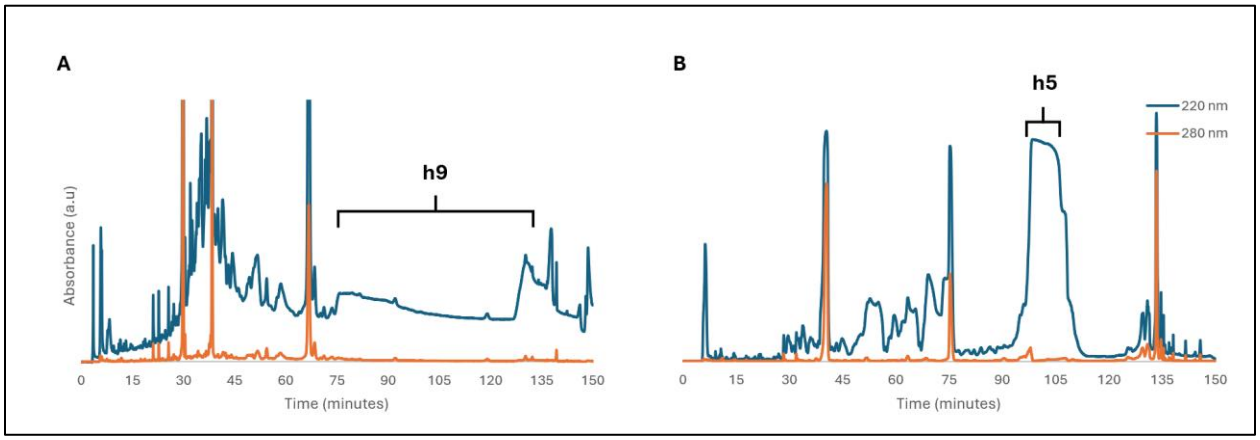

Figure 12: Preparative purification of peptides using TFA-containing mobile phases. (A) HPLC chromatogram of h5 peptide purification. (B) HPLC chromatogram of h9 peptide purification.

To reduce the hydrophobicity of h9 peptides in solution, TFA was substituted with a more hydrophilic formic acid counterion. Substitution of TFA with formic acid was observed to reduce

h9 crude product retention times by approximately 10 minutes during a 2%/min gradient elution (Fig. 13).

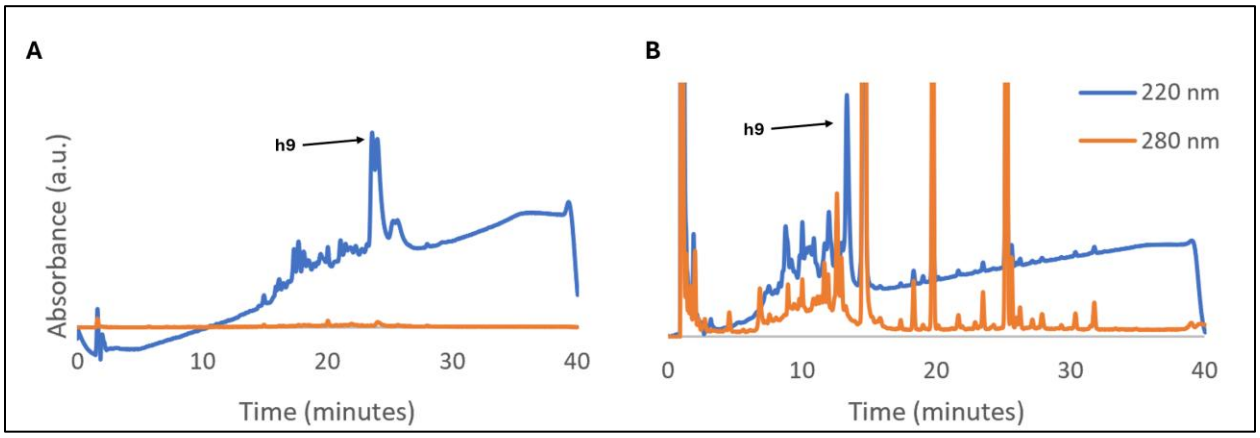

Figure 13: Effect of acid-counterion on peptide purification. HPLC chromatograms of crude h9 peptides eluted with (A) TFA-containing mobile phases and (B) Formic acid-containing mobile phases. Both analyses were performed via gradient elution from 20-80% CAN/H20 over 30 minutes, followed by a 10 minute wash cycle.

To obtain pure peptides, fractions containing minimal 280 nm absorbances were collected, pooled, and sent for analysis via mass spectrometry (Fig. 14).

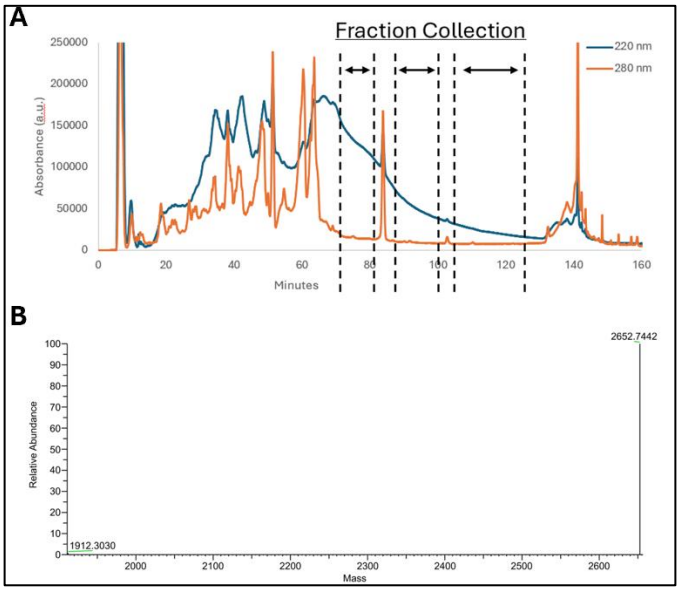

Figure 14: Purified peptide fractionation. (A) Preparative HPLC chromatogram and fractionation and (B) resulting mass spectrum of purified fractions.

2.2.5 Purity Coefficient Determination

BAPCs are often assembled at µL volumes with µM concentrations. As a result, µg amounts of peptides must be aliquoted. It is impractical to weigh these amounts and thus spectral absorbance of peptide bonds, or preferably aromatic residues, are used to measure concentration before aliquoting. As seen in previous figures, impurities can account for high percentages of sample UV absorbance. Even after purification, small concentrations of impurities may persist and have varying degrees of effect on UV absorbance. To accurately measure sample peptide concentrations, I opted to re-analyze purified products and signal impurities at wavelengths used downstream for concentration determination and generate a coefficient of target peptide signal purity by integrating signal peaks (Fig. 15). Singal purity coefficients often range from 30-99%.

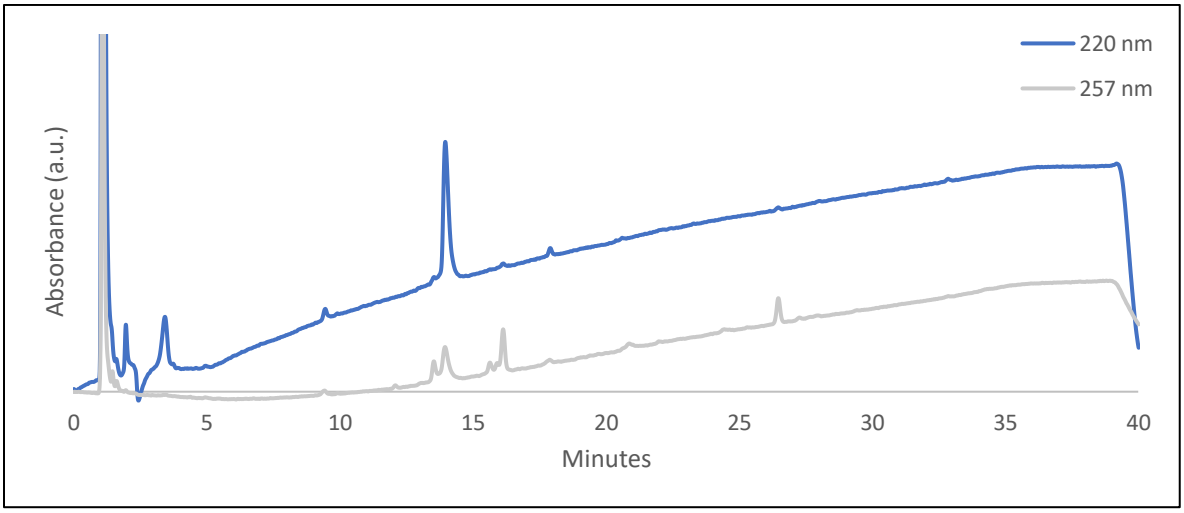

Figure 15: Peptide spectral purity coefficient determination. Purified h9 peptide was analyzed for signal purity at 220 nm and 257 nm, resulting in a 257 nm signal purity coefficient of 43.89%.

2.2.6 BAPC-mRNA condensation

To investigate the interaction of purified BAPs with nucleic acids and explore differences in comparison to impure BAPs, nucleic acid-BAPC complexes from varying batches were assayed via gel retardation. At low N:P ratios, free mRNA was observed stained, migrating into an

agarose gel (Fig. 16). At high N:P ratios, condensed mRNA was stained and remained in the well, likely resultant from complexation with BAPC complexes too large to enter the gel matrix. The condensation ratio for pure peptides, inclusive of a concentration correction coefficient was observed to be around an N:P of 2.5. Interestingly, a similar ratio was observed for impure peptides generated via our original protocols and sourced from Kansas State.

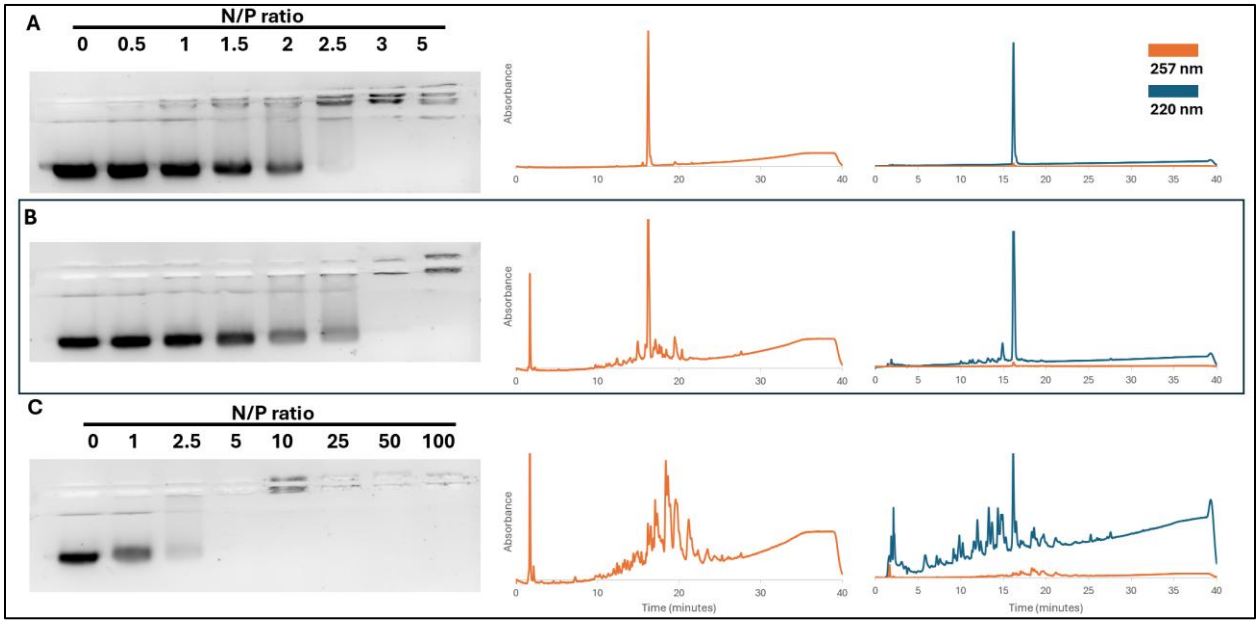

Figure 16: BAPC-mRNA condensation. Gel retardation assays and chromatograms of assayed h5 peptides of (A) pure peptides (B) Kansas State peptides and (C) peptides synthesized before optimizatiton.

2.2.7 BAPC-mRNA complex size

To validate the interaction between our BAPs and nucleic acids and to assess the formation and stability of BAPCs and BAPC-nucleic acid complexes, I analyzed BAPCs and BAPCs complexed with mRNA at an N:P ratio of 11 over several weeks via atomic force microscopy (AFM) (Fig. 17). BAPCs were observed to form majority small, 10-40 nm nanoparticles. Upon addition of mRNA, these nanoparticles were observed to assemble into larger nanoparticles on the range of 100-300 nm (Fig. 17A). Nanoparticles and mRNA complexes were observed to

remain stable for two weeks when refrigerated at 4℃ before transitioning into apparent nanofibril-like structures. Quantitative analysis showed the majority of nanoparticles in BAPC-only and BAPC-mRNA samples to be sized below 50 nm (Fig. 17B). While the addition of mRNA induces the formation of larger nanoparticle clusters, the majority of nanoparticles likely remain small due to the number of BAPCs being greater than the amount required to condense the total mRNA in solution resultant from an N:P ratio of 11.

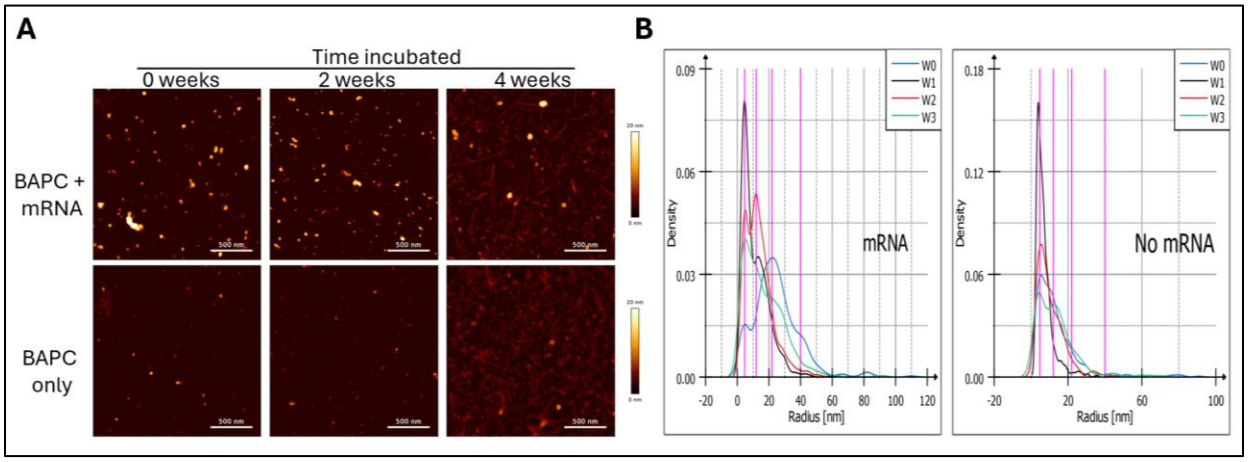

Figure 17: BAPC/BAPC-mRNA size and stability. (A) Representative AFM images of BAPCs and BAPC-mRNA complexes over a 4-week period. (B) Statistical analysis of radii of BAPCs particles with and without mRNA at weekly interval. The four lines on both panels correspond to 4.7 nm, 12 nm, 22 nm, and 40 nm.

2.3 Conclusions

With this chapter, I have outlined BAP synthesis, purification, and assembly protocols, and impressed the importance of batch quality control. BAPs can be readily synthesized via SPPS. Following synthesis, BAPs of varying hydrophobicity can be analyzed and purified via reverse phase chromatography on C-18 columns. Purified peptides, however, often contain small impurities with significant effects of spectral purity and subsequent BAPC concentrations. Correctly analyzed BAP products can be assembled into BAPCs which predominantly form small 10-40 nm nanoparticles. BAPs containing significant spectral or peptide impurities may

result in large differences in measured concentrations, and subsequent BAPC-RNA interactions. Upon the addition of mRNA, these nanoparticles cluster into BAPC-mRNA complexes with larger 100-300 nm sizes. BAPCs and BAPC-mRNA complexes are then stable for up to 2 weeks at 4℃, and transition to fibril conformation after four weeks incubation at 4℃.

Chapter 3: *In Vitro* Transfection and Toxicity

3.0 Introduction

Gene delivery nanoparticle efficacy involves two key measurements of transfection efficiency and toxicity. Nanoparticles must be able to efficiently deliver RNA therapeutics and do so without damaging cells to a target's detriment. It should be noted that some cellular damage and toxicity may be preferred and/or designed into a nanoformulation; one such example if the ionizable lipid component of the Moderna mRNA vaccine.[41–43] Ionizable lipid ALC-0315 has been reported to activate innate immune responses and induce inflammation.[44] In the case of vaccination however, this outcome is ideal as it helps to activate adaptive immunity which is essential to vaccination.

In vitro, many organic and inorganic nanoparticles have been reported to have toxicities related to their size, charge, and components (Fig. 18).[45,46] Small nanoparticles are readily taken up via endocytosis, pinocytosis, micropinocytosis, and phagocytosis. Once inside the cell, nanoparticles may induce toxicity via formulation-specific mechanisms, or steric inhabitance of intracellular movements and organelles.[45,46]

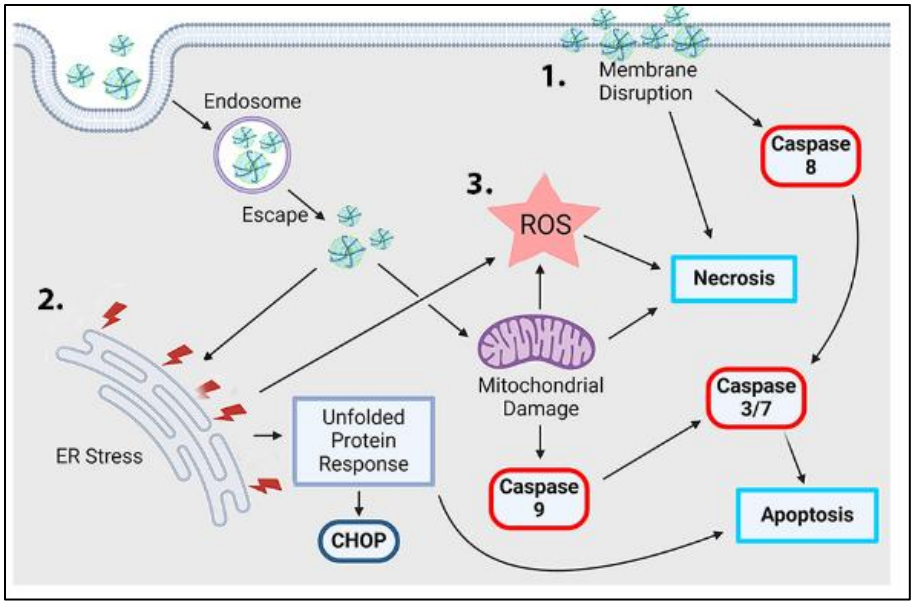

Figure 18: Mechanisms of cellular toxicity. (A) Schematic representation of toxicity pathways induced by nanoparticles (NPs), including the intrinsic (1, 2) and extrinsic (3) apoptotic pathways (toxicity readouts are highlighted in *color)*

Positively charged nanoparticles have been reported to interact with cellular membranes and induce toxicological effects via membrane disruption and the inhibition of cell-surface proteins.[47,48] Inside of the cell, charged nanoparticles can also induce inflammatory responses via innate immune mechanisms.[44] Positively charged nanoparticles have also been reported to interfere with mitochondrial and endosomal membranes, potentially resulting in the release and/or induction of reactive oxygen species.[48] Intracellular charged species may also interact with proteins to the detriment of homoeostasis.

Transfection efficiency can be evaluated in several ways depednent on the type of nucleic acid being delivered. For mRNA encoding fluorescent proteins, cells can often be analyzed via flo cytometry or light microscopy. Non-fluorescent proteins can be quantified via antibody staining; western blot can be performed, or fluorophore-tagged antibodies can be incubated with cells to conduct live-cell staining and imaging. siRNA transfection can be evaluated via the same methods, with efficiency being quantified by a reduction in protein expression in treated cells compared to controls.

In this section, I assay the transfection efficacy of purified h5/h9 BAPCs complexed with GFP-encoding mRNA or anti-GFP siRNA. Mamalian cells constitutively expressing GFP are silenced via siRNA transfection, while non-expressive mamalian cells are transfected wth GFP mRNA. Cytotoxicity associated with BAPC-mRNA complex transfection is then investigated. Specifically, I investigate mechansisms which might result in poor transfection efficiency, or inhibition of RNA expression, including apoptosis and necrosis, ER stress, and mitochondrial and metabolic disfunction.

3.1 Materials and Methods

3.1.1 Materials

5-methoxyuridine modified GFP mRNA (TriLink BioTechnologies Inc. San Diego, CA, USA), Herringbone micromixer (Darwin Microfluidics, Paris, France), 2,2,2-Trifluoroethanol (TFE) (Tokyo Chemical Industry Ltd), snakeskin MWCO 12000-14000 Da dialysis tubing (Themo fisher scientific, Waltham, MA), DSPC (Sigma-Aldrish, Co., St. Louis, MO 63103), Cholesterol (Echelon Biosciences, Salt Lake City, UT 84108), ALC-0315 (MedChemExpress, Monmouth Junction, New Jersey), DMG-PEG2000 (Avanti Polar Lipids, Alabaster, Alabama 35007), HRP conjugated goat anti-mouse (405-306, Biolegend, San Diego, CA, USA), 96-well plate (Brand immunograde, Brand GmbH, Wertheim, Germany #781722), Tween-20 (Themo fisher scientific, Waltham, MA), flow cytometer MACSQuant® Analyzer 10 (Miltenyi Biotec, Germany).WI-38, RAMOS, CHO and NIH-3T3 cells (ATCC). CellQuanti-Blue Cell Viability Assay Kit (biotrend, USA), Cell Meter Muliplexing Capsase 3/7, 8, and 9 Activity Assay Kit (AAT Bioquest, USA), Mouse Anti-CHOP/DDIT3 antibody (Catlogue # ab11419), CellROX Deep Red Reagent (ThermoFisher, USA), Pacific Blue Annexin V Apoptosis Detection Kit with PI (BioLegend, USA), Staurosporine (ThermoFisher, USA), Thapsigargine (Ambeed, USA).

3.1.2 Transfections

CHO or GFP-expressing CHO cells were seeded at 50,000 cells/mL into 12 well plates. After 24 hours incubation, NT groups were treated with saline, PP groups were treated with PolyPlus JetMessenger + 1 ug mRNA or PolyPlus Interferin + 1 ng siRNA at product specified-ratios, BAPC-RNA groups were treated with BAPCs complexed with either 1 ug mRNA or 1 ng siRNA at N:P 11, and BAPC only groups were treated with the concentration of BAPCs used with BAPC-RNA groups without the addition of RNA. Cells treated with mRNA were analyzed 24 hours after treatment, and cells treated with siRNA were analyzed after 48 hours. Cells treated with fluorescent BAPCs were dosed with concentrations of BAPCs equivalent to those required for the siRNA transfections described above.

3.1.3 Formation of BAPCs and BAPC-mRNA Complexes

Two peptides, bis(Ac-FLIVI)-K-K_4 and bis(Ac-FLIVIGSII)-K-K_4, were synthesized by solid phase peptide chemistry as previously described [49]. Each peptide was dissolved separately in TFE and molar concentrations were determined by the absorbance of phenylalanine at 257.5 nm ($\varepsilon = 195$). Both peptides were mixed at equimolar ratios and dried using Centrivap Vacuum Concentrator (Labconco). BAPCs were formed by resuspending peptides in sterile deionized (dI) H_2O and incubated for 10 minutes at 25°C. The solution was then cooled to 4°C for 1 h to prevent BAPCs fusion.[26] Finally, BAPCs were mixed at N:P 11 with 5-methoxyuridine modified luciferase or Ova mRNA and vortexed for 10 seconds. The N:P ratio was calculated by dividing the number positively charged peptide amines by the number of negatively charged phosphate groups of the added mRNA backbone. Cyanine3-labeled BAPCs were prepared at a peptide ratio of 3% Cyanine3-labeled h5 : 47% h5 : 50% h9.

3.1.4 LNP Synthesis

Lipid nanoparticles were prepared via ethanol dilution through a Y-shaped, staggered herringbone micromixer. Lipid stocks were prepared containing 8 mg/mL 10:38.5:50:1.5 molar ratio DSPC: Cholesterol: ALC-0315: DMG-PEG2000 in 100% ethanol. 100 mM citrate buffer containing mRNA at pH 3-4 was used as an aqueous phase. For dilution, aqueous and organic phases were combined at 0.75 and 0.25 mL/min respectively using separate NE-1000 one channel programmable syringe pumps. LNP-mRNA complexes were prepared at N:P 5.1, where N was the number of positively charged lipid amines and P was the number of negatively charged phosphate groups of the added mRNA backbone. Following dilution, LNPs were dialyzed using snakeskin, dialysis tubing (MWCO 12000-14000 Da) for 16h under magnetic stirring against a 1000X volume of PBS.

3.1.5 In vitro Toxicity

WI-38, NIH-3T3, and RAMOS cells were incubated with 1 μM staurosporine, 0.2 μM thapsigargine, BAPC-Ova, or LNP-Ova for 24h and then analyzed. Cellular viability was assessed using CellQuanti-Blue Cell Viability Assay Kit. Apoptosis/Necrosis staining was performed using Pacific Blue Annexin V Apoptosis Detection Kit with PI. ROS concentrations were quantified via staining with CellROX Deep Red Reagent. DDIT3/CHOP protein was detected using antibodies from Abcam. Caspase detection was performed using Cell Meter Multiplexing Caspase 3/7, 8, and 9 Activity Assay Kit.

3.2 Results and Discussion

3.2.1 BAPC-RNA Transfection

BAPCs constructed from purified h5 and h9 peptides were assessed for their transfection efficacy complexed with mRNA and siRNA at N:P ratio 11. N:P 11 has previously been reported efficacious *in vivo* during preliminary vaccine trials when complexed with OVA-mRNA and will be used throughout the rest of this section. GFP was used as a reporter for transfections, and efficacy was assessed by variation in FITC fluorescence between groups. Chinese hamster ovary (CHO) cells were treated with translatable BAPC-GFP mRNA complexes while a GFP-expressive CHO cell line was treated with BAPC-GFP siRNA complexes. Insignificant or zero rates of transfection were observed with all groups of BAPCs and nucleic acid complexes (Fig. 19A, B).

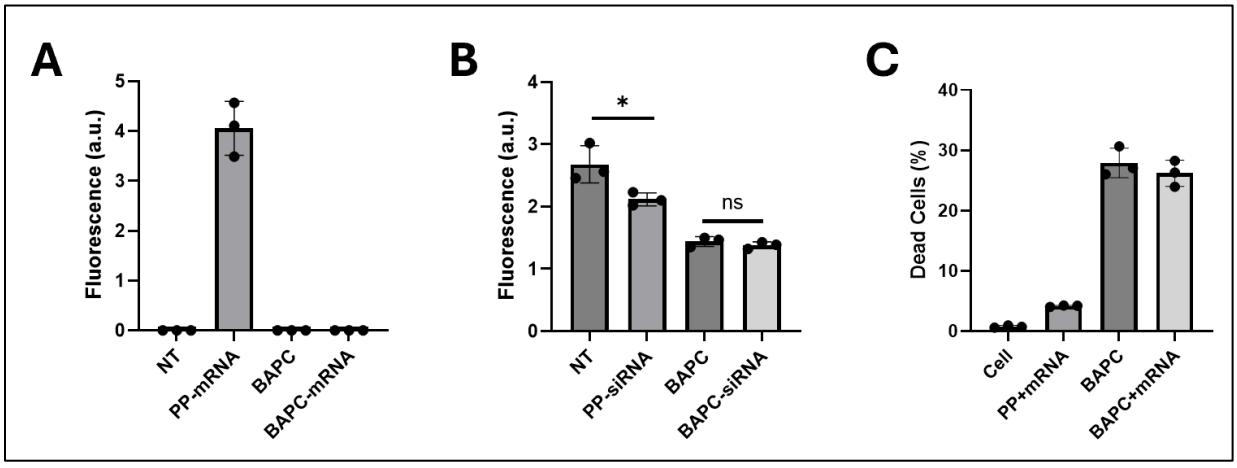

Figure 19: BAPC-RNA transfection. (A) Transfection of CHO cells with GFP-mRNA. (B) Transfection of GFP-expressive CHO cells with anti-GFP siRNA. (C) Viability of cells transfected with GFP-mRNA. Data was analyzed with t tests. Non-statistical significance (ns) was considered when $p > 0.05$, (*) $p < 0.05$.

When observed via flow cytometry in the presence of a membrane-impermeable viability dye, autofluorescent cells were found to have permeable membranes (Fig. 19C). GFP-expressing CHO cells treated with BAPCs and BAPC-siRNA complexes were also found to have significantly reduced GFP expression. Together, the elevated incidence of membrane

permeability and decreased gene expression may indicate cellular toxicity of BAPCs and BAPC-mRNA complexes.

The absence of measurable transfection was unexpected, especially given the success of BAPCs *in vivo*. When compared to lipid nanoparticles, for example, BAPCs proved equally efficacious as mRNA vaccine delivery vectors in C57BL/6 albino mice by measure of IgG antibody induction (Fig. 20).[35] Given this measure and other examples of the efficacy of purified BAPCs as *in vivo* RNA delivery vectors, I hypothesized that BAPCs might be causing toxicity at *in vitro* concentrations or in *in vitro* cell types, inhibiting RNA expression and/or preventing transfection.

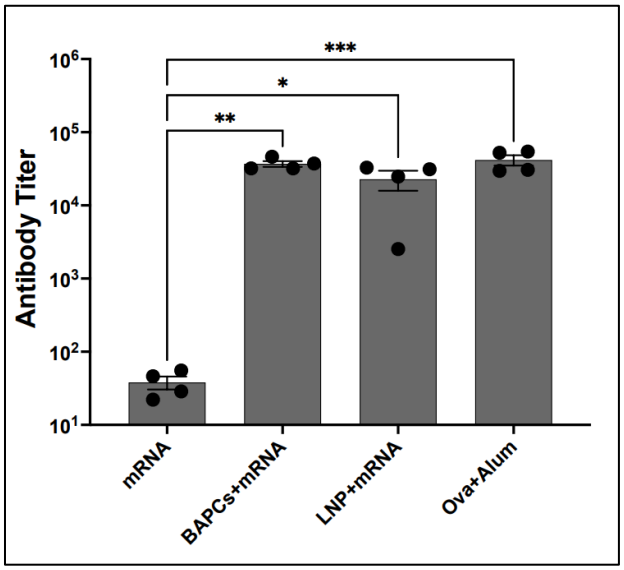

Figure 20: Anti-OVA antibody responses in C57BL/6 mice. Animals immunized intramuscularly using alum-ovalbumin, ovalbumin mRNA, BAPC-mRNA and LNP-mRNA plus PBS and BAPCs only as a negative control (data not plotted). (each dot on a plot represents a data from individual animal) (mean ± SEM, n = 4). Differences between values were compared by ANOVA using Tuckey as post-test. Statistical significance: (*) $p < 0.05$, (**) $p < 0.01$; (***) $p < 0.001$. Non-statistical significance (ns) was considered when $p > 0.05$.[35]

3.2.2 Morphology

To investigate BAPC toxicity as a potential inhibitor of gene expression of transfected complexes, I analyzed 24-h acute BAPC-induced morphological changes in CHO cells treated

with fluorescently-labeled BAPCs, with the 24-h time point corresponding to the analysis timepoint of mRNA-treated cells in section 3.2.1. After 24 hours, BAPC complexes can be observed to induce vacuole-like formations within cells. When treated with fluorescent, Cyanine3-labeled BAPCs, these vacuoles appear to fluoresce; additionally, BAPCs appear to coat cellular membranes (Fig. 21).

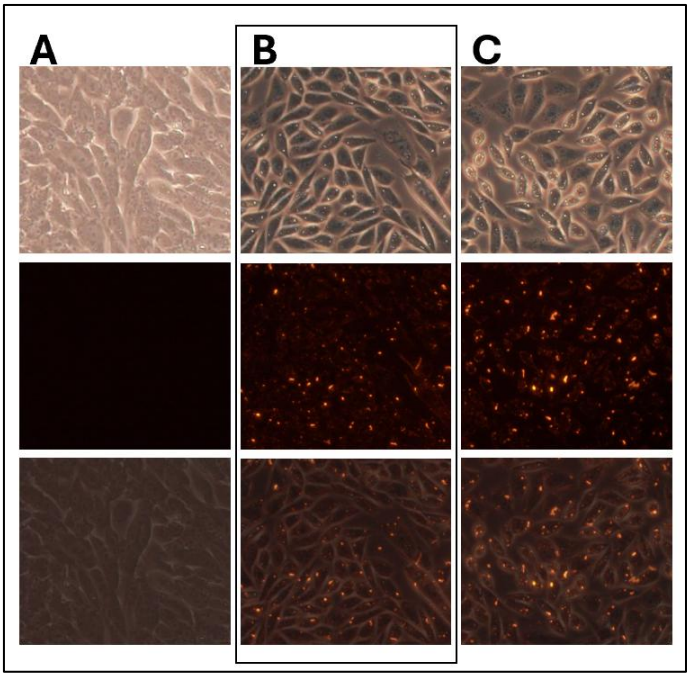

Figure 21: Morphology of BAPC-treated cells. CHO cells treated with (A) PBS and (B, C) fluorescent BAPCs. Brightfield (top row), TRITC (middle row), and brightfield/TRITC overlay (bottom row).

3.2.3 General Viability

To investigate metabolic activity and general cellular viability, I assayed the effects of varying concentrations of BAPCs and BAPC-mRNA complexes on cellular metabolic activity. Additionally, as a comparison and given our recent work towards developing BAPCs as a vaccine vector, I opted to include empty and RNA-complexed LNPs as additional groups for comparison. I initially screened a wide range of BAPC and LNP concentrations (1–50 μg/mL),

using the resazurin assay (Fig. 22). Here, and for the following sections 3.2.4-3.2.8, I report results obtained with NIH-3T3 cells. While results were also repeated in CHO cells, NIH-3T3 cells are mouse fibroblasts, and represent a cell type which BAPC-RNA complexes might interact with during *in vivo* intramuscular (IM) injection. Using NIH-3T3 cells additionally allows us to compare our *in vitro* results to toxicity data obtained *in vivo* through murine model IM injections. Results for CHO cells as well as human fibroblast WI-38 cells are reported in Appendix A.

As seen in Figure 22, 10 µg/ml, which corresponds to our treatment concentrations for sections 3.2.1-3.2.2, showed an approximate 20% reduction in viability for both BAPC-mRNA and LNP-mRNA groups in comparison to no treatment. Interestingly, BAPCs did not show a significant departure from LNPs with regards to transfected-cell metabolic activity.

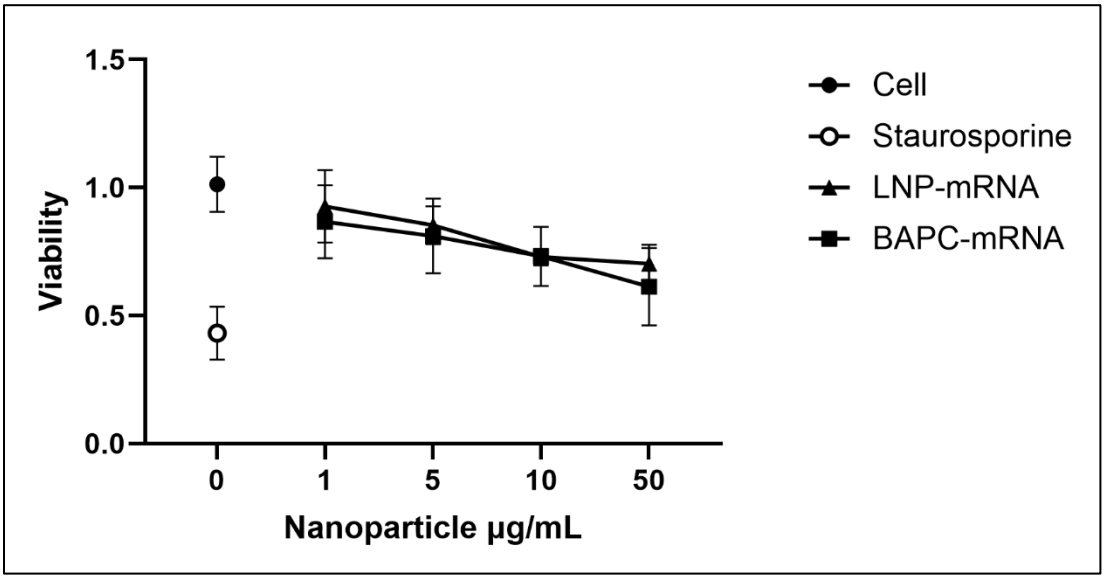

Figure 22: General Viability. NIH-3T3 cells were incubated for 24 hours with varying concentrations of BAPCs and LNPs, while maintaining nanoparticle ratios of 11 and 5.1, respectively. Cellular viability was then assessed using a resazurin assay. Statistical analysis revealed that the P-values comparing LNP-mRNA, BAPC-mRNA at 10 µg, and the cell-only control were (*) $p < 0.05$.

3.2.4 Apoptosis and Necrosis

To determine whether the viability reduction observed in Figure 22 was due to cell death via apoptosis or necrosis, I assessed these pathways using annexin V/propidium iodide staining (Fig. 23). Treatment of NIH-3T3 cells with 10 µg/mL with BAPCs-mRNA groups led to increased apoptotic and necrotic cells compared to both the no-treatment and LNP-mRNA groups. Nevertheless, I hypothesized that this effect might be partially attributable to the mechanical stress induced during cell detachment. BAPC-treated cells often require more vigorous pipetting for detachment due to the cationic nature of the material, and I speculated that the observed apoptosis and necrosis could be a consequence of cellular damage induced by the mechanical stress during detachment. When the experiment was repeated with suspension Ramos cells and NIH-3T3 no significant difference in apoptosis or necrosis was observed (Supp. Fig. 5).

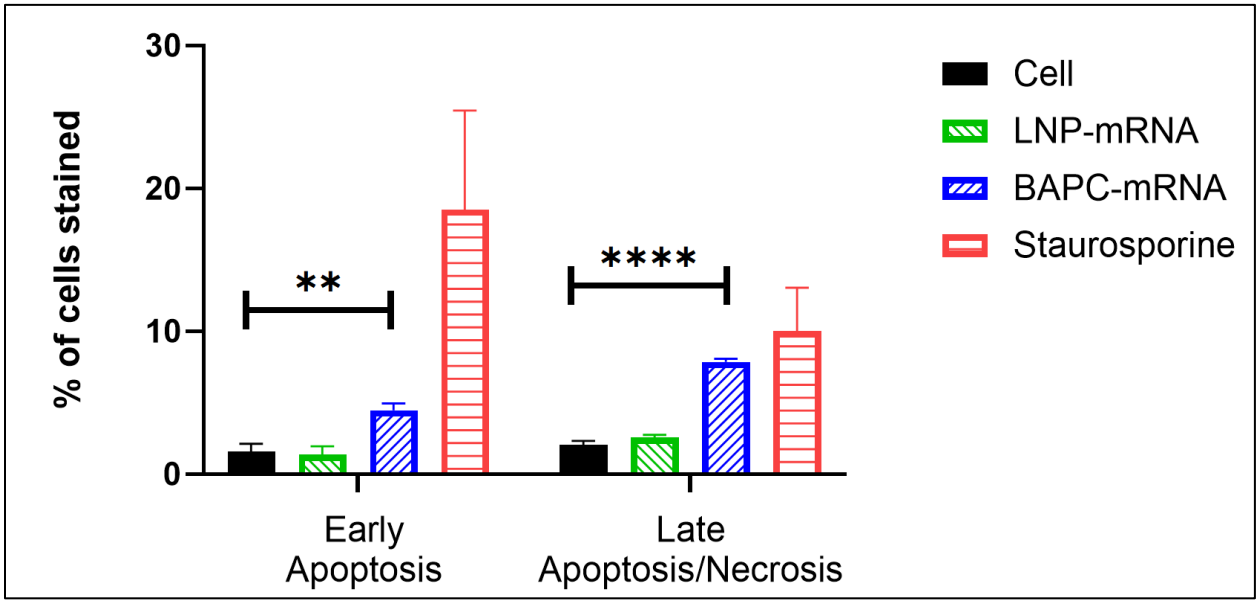

Figure 23: Apoptosis/necrosis. Annexin/PI staining of NIH-3T3 cells after 24-h incubation with 10 µg/mL BAPC-mRNA or LNP-mRNA. Data was analyzed with t tests. (**) $p < 0.01$ and (****) $p < 0.0001$. Non-statistical significance (ns) was considered when $p > 0.05$.

3.2.5 Caspase 3/7 Activation

Toxicity resulting in programmed cell death often results in the induction of caspases – a family of 12 cysteine proteases responsible for driving and enacting programmed cell death.[50,51] They are categorized into two major groups: initiator caspases (which activate downstream executioner caspases) and executioner caspases (which carry out the final steps of apoptosis or cell death). Caspases 3 and 7 are executioner caspases, and their detection would imply that cells are undergoing apoptosis in response to nanoparticles. Treatment of NIH-3T3 cells showed minimal activation of caspases 3 and 7, indicating BAPC do not significantly induce late-stage, caspase-mediated apoptosis and cell death, supporting our hypothesis that toxicity observed in BAPC-mRNA treated groups may have been due to the additional mechanical stress necessitated during the assay (Fig. 24).

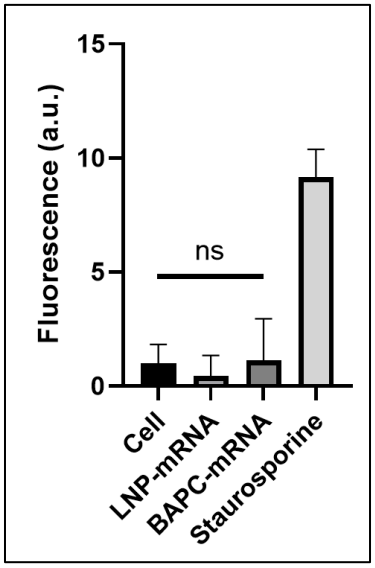

Figure 24: Caspase 3/7 Activation. Activation of caspase 3 or 7 in NIH-3T3 cells after 24-h incubation with 10 μg/mL BAPC-mRNA or LNP-mRNA. Data was analyzed with t tests. Non-statistical significance (ns) was considered when $p > 0.05$.

3.2.6 CHOP Activation

The endoplasmic reticulum (ER) is responsible for lipid and peptide synthesis. Disruptions of the ER can lead to an accumulation of unfolded proteins.[50] Due to LNP and BAPC nanoparticles being composed of lipids and peptides, I chose to investigate ER stress as a potential avenue of toxicity and metabolic inhibition as well. ER stress can result in activation of the unfolded protein response, detectable by upregulation of the CHOP/DDIT3 transcription factor[52]. As seen in Figure 25, DDIT3/CHOP protein was not detectable in groups treated with 10 µg/mL of either BAPC-mRNA or LNP-mRNA complexes. Analogous results were seen in WI-38 fibroblast as well (Supp. Fig. 3).

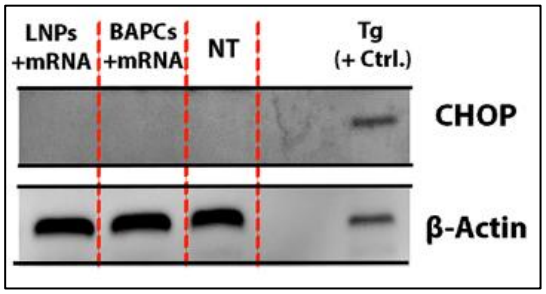

Figure 25: CHOP/DDIT3 activation. ER stress induced by treatment of cells with LNP-mRNA and BAPC-mRNA complexes or thapsigargine as measured by western blot analysis of CHOP/DDIT3 expression.

3.2.7 ROS Activation

Nanoparticles have also been observed capable of inducing the generation and/or release of reactive oxygen species, such as superoxide, hydrogen peroxide, and hydroxyl radicals, through damage to endosomal compartments, organelles, and other mechanisms. The cytoplasmic release of these radicals can oxidize proteins, DNA, lipids, and other biomolecules with detrimental effects, ultimately resulting in cellular viability reduction, apoptosis, or necrosis.[53] No significant ROS generation was observed in the BAPC-mRNA and LNP-mRNA treatment groups compared to the untreated controls in both NIH-3T3 and WI-38 cells (Fig. 26, Supp. Fig. 3).

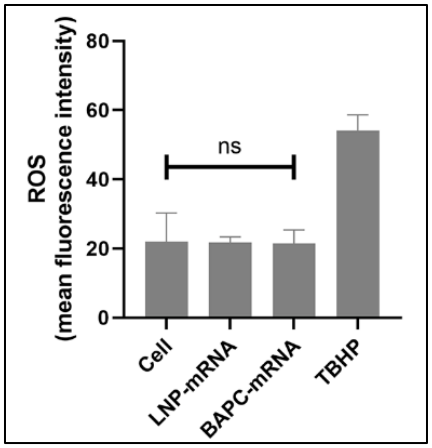

Figure 26: Total ROS generation. Acute toxicity induced by 24h incubation with 10 µg/mL BAPC-mRNA or LNP-mRNA Complexes in a NIH-3T3 cells. Data was analyzed with t tests. Non-statistical significance (ns) was considered when $p > 0.05$.

3.3 Conclusions

BAPCs made from purified h5 and h9 BAPs are ineffective at transfecting mRNA and siRNA *in vitro* at N:P 11, which was previously reported as efficacious *in vivo* with BAPC-mRNA complexes. Investigating toxicity as a potential cause of poor transfection, BAPCs do not appear to induce reactive oxygen species or ER-related stress. However, increasing concentrations of BAPC treatments does reduce the viability of cells. Groups of cells treated with BAPCs display higher rates of membrane permeability, apoptosis, and necrosis than cells treated with LNPs or saline. Fluorescently-labeled BAPCs appear to adhere to cellular membranes and induce vacuole formation within cells. It is therefore likely that BAPCs induce membrane-related stress to cells, likely interacting through electrostatic interactions to disrupt or inhibit cellular membranes, increasing cellular permeability and reducing function and viability. Similar incidence of membrane-associated toxicity have been reported for other highly-cationic nanoparticles.[47]

Conclusions and Future Directions

Conclusions

With this publication, standardized methods for the synthesis, purification, and assembly of branched amphiphilic peptides and capsules are made available, which will allow for the widespread replication of BAPC technology and research. Individual BAP residue coupling times should be optimized, and impurities resulting from resin cleavage or side chain reactions should be eliminated to improve crude yields. BAPs should then be purified via reverse-phase C18 or other chromatography to obtain pure species. The significant variability of BAPC-RNA interactions and concentrations between pure and impure BAPC peptides was also impressed, outlining the importance of batch quality for experimentation and high-fidelity research. Impurities present in batches of crude or insufficiently purified BAPs may have substantial extinction coefficients at wavelengths used for BAPC aliquoting and result in measured concentrations orders of magnitude greater than the actual peptide concentration in subsequent BAPC aliquots. Shortened peptide impurities also appear to have a much greater ability to condense RNA than full length h5 and h9 peptides.

BAPCs constructed from purified BAPs were found not efficacious at mRNA or siRNA delivery *in vitro* when complexed with RNA at N:P 11. At this N:P ratio, BAPCs induced non-specific, membrane-interaction associated toxicity, either inducing cell death via apoptosis or necrosis, or inhibiting RNA expression. BAPCs were not found to induce ROS generation or ER stress, and

were found to result in similar levels of general metabolic toxicity to LNPs when treated at elevated concentrations.

Moving forward, BAP sequence modifications should be made to facilitate lower cellular toxicity and increased transfection efficacy *in vitro*. Being composed of amino acids, BAPCs have an abundant source of amino acid diversity to include in modifications. Furthermore, because BAPs are produced synthetically, non-canonical amino acids may be used. Ionizable, aromatic, and other amino acids can each be individually leveraged to alter charge, UV-absorption, nanoparticle stability, and other aspects.

Future Directions

Several avenues for BAP development present themselves when investigating commercially available LNP technology. LNPs make use of ionizable lipids to reduce surface charge, increase stability in serum, and reduce cellular toxicity. Peptide sequences containing the ionizable amino acid histidine could be made for this purpose. Ionizable lipids may also be important for cellular entry. As outlined in Figure 1, the proton sponge effect and the inclusion of buffering capacity into a nanoformulation may serve to increase endosomal escape. Amino acids such as histidine with a pK_as relevant to the endolysosomal environment may significantly enhance BAPC endosomal escape.

The success of BAPC-dsRNA complexes as oral delivery vectors in insect models may be in part due to lysine residues gaining buffering capacity. Insect guts have been reported with pHs at or around the pK_a of lysine (~10.54).[54] It is possible that within insects, BAPCs gain buffering capacity, facilitating improved endosomal escape and intracellular RNA expression.

BAPCs also suffer from size heterogeneity. While complexes can be stabilized via refrigeration at 4°C, populations as seen in Figure 17 remain heterogeneous. Microfluidics could be used to isolate uniformly sized populations of BAPCs. Indeed, when BAPC complexes are dissolved into 40% TFE/H_2O and then diluted at a 1:3 ratio into three parts pure H_2O through a herringbone mixer, uniform and homogenous populations of BAPCs can be obtained as analyzed via dynamic light scattering (Fig. 27). Issues with microfluidic assembly and trifluoroethanol dilution may include sizing and rapid fusion of BAPCs, however this can be mediated by the inclusion of PEGylated lipids such as DMG-PEG2000. Amino acid alternatives to PEG such as sarcosine may be explored.

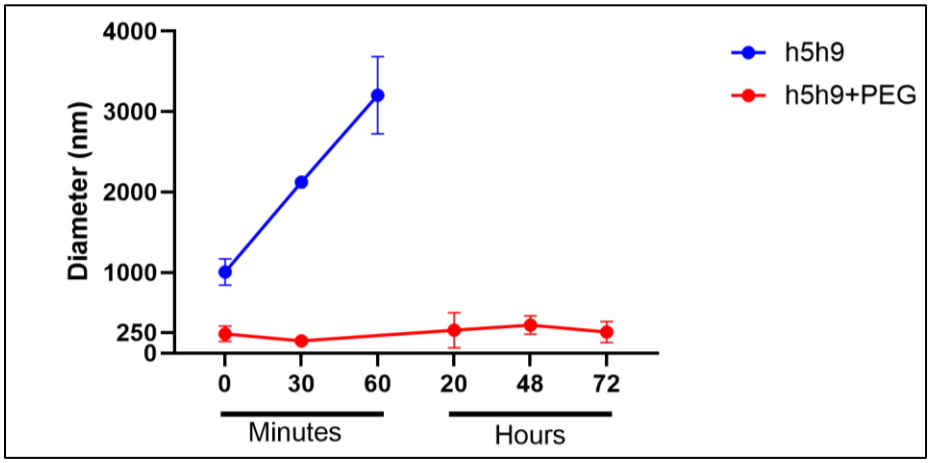

Figure 27: BAPC Microfluidic and PEGylated Synthesis. BAPCs composed of 50/50 h5 and h9 peptides or 49/49/2 h5/h9/DMG-PEG2000 formed via microfluidics. Time points were analyzed after incubation at room temperature.

References

(1) DeLong, R. Ushering in a New Era of RNA-Based Therapies. *Communications biology*. 2021. https://doi.org/10.1038/s42003-021-02150-w.

(2) Chakraborty, C.; Sharma, A. R.; Sharma, G.; Doss, C. G. P.; Lee, S.-S. Therapeutic MiRNA and SiRNA: Moving from Bench to Clinic as Next Generation Medicine. *Mol Ther Nucleic Acids* **2017**. https://doi.org/10.1016/j.omtn.2017.06.005.

(3) Alnylam Pharmaceuticals, I. *https://www.onpattrohcp.com/how-onpattro-works*. https://www.onpattrohcp.com/how-onpattro-works.

(4) HEART UK. *https://www.heartuk.org.uk/getting-treatment/inclisiran*. https://www.heartuk.org.uk/getting-treatment/inclisiran.

(5) Alnylam Pharmaceuticals, Inc. *https://www.givlaari.com/what-is-givlaari*. https://www.givlaari.com/what-is-givlaari.

(6) Prior, I. A.; Lewis, P. D.; Mattos, C. A Comprehensive Survey of Ras Mutations in Cancer. *Cancer Res* **2012**, *72* (10), 2457–2467. https://doi.org/10.1158/0008-5472.CAN-11-2612.

(7) M.D. Anderson Cancer Center. *IExosomes in Treating Participants with Metastatic Pancreas Cancer with KrasG12D Mutation*; Houston, 2024.

(8) Cuciniello, R.; Filosa, S.; Crispi, S. Novel Approaches in Cancer Treatment: Preclinical and Clinical Development of Small Non-Coding RNA Therapeutics. *J Exp Clin Cancer Res* **2021**, *40* (1), 383. https://doi.org/10.1186/s13046-021-02193-1.

(9) Bartoli, A.; Gabrielli, F.; Tassi, A.; Cursaro, C.; Pinelli, A.; Andreone, P. Treatments for HBV: A Glimpse into the Future. *Viruses* **2021**, *13* (9). https://doi.org/10.3390/v13091767.

(10) Braga, A. C. S.; Carneiro, B. M.; Batista, M. N.; Akinaga, M. M.; Rahal, P. Inhibition of Hepatitis C Virus Using SiRNA Targeted to the Virus and Hsp90. *Cell Stress Chaperones* **2017**, *22* (1), 113–122. https://doi.org/10.1007/s12192-016-0747-8.

(11) Drinnenberg, I. A.; Weinberg, D. E.; Xie, K. T.; Mower, J. P.; Wolfe, K. H.; Fink, G. R.; Bartel, D. P. RNAi in Budding Yeast. *Science* **2009**, *326* (5952), 544–550. https://doi.org/10.1126/science.1176945.

(12) Moazeni, M.; Khoramizadeh, M. R.; Kordbacheh, P.; Sepehrizadeh, Z.; Zeraati, H.; Noorbakhsh, F.; Teimoori-Toolabi, L.; Rezaie, S. RNA-Mediated Gene Silencing in Candida Albicans: Inhibition of Hyphae Formation by Use of RNAi Technology. *Mycopathologia* **2012**, *174* (3), 177–185. https://doi.org/10.1007/s11046-012-9539-6.

(13) ARCTURUS Therapeutics. *Arcturus Therapeutics Announces Initiation of Dosing in Phase 2 Multiple Ascending Dose Studies for Cystic Fibrosis (CF) and Ornithine Transcarbamylase (OTC) Deficiency*. https://ir.arcturusrx.com/.

(14) Liu, C.; Zhou, Q.; Li, Y.; Garner, L. V; Watkins, S. P.; Carter, L. J.; Smoot, J.; Gregg, A. C.; Daniels, A. D.; Jervey, S.; Albaiu, D. Research and Development on Therapeutic Agents and Vaccines for COVID-19 and Related Human Coronavirus Diseases. *ACS Cent Sci* **2020**. https://doi.org/10.1021/acscentsci.0c00272.

(15) Carly (Kempler) Pflaum. FDA Approves First Gene Therapies to Treat Patients with Sickle Cell Disease. *FDA*. December 8, 2023.

(16) Aldosari, B. N.; Alfagih, I. M.; Almurshedi, A. S. Lipid Nanoparticles as Delivery Systems for RNA-Based Vaccines. *Pharmaceutics*. 2021. https://doi.org/10.3390/pharmaceutics13020206.

(17) Kowalski, P. S.; Rudra, A.; Miao, L.; Anderson, D. G. Delivering the Messenger: Advances in Technologies for Therapeutic MRNA Delivery. *Molecular Therapy*. 2019. https://doi.org/10.1016/j.ymthe.2019.02.012.

(18) Lamson, N. G.; Fein, K. C.; Gleeson, J. P.; Newby, A. N.; Xian, S.; Cochran, K.; Chaudhary, N.; Melamed, J. R.; Ball, R. L.; Suri, K.; Ahuja, V.; Zhang, A.; Berger, A.; Kolodieznyi, D.; Schmidt, B. F.; Silva, G. L.; Whitehead, K. A. The Strawberry-Derived Permeation Enhancer Pelargonidin Enables Oral Protein Delivery. *Proc Natl Acad Sci U S A* **2022**, *119* (33), e2207829119. https://doi.org/10.1073/pnas.2207829119.

(19) Yuhua, L.; Kunyuan, G.; Hui, C.; Yongmei, X.; Chaoyang, S.; Xun, T.; Daming, R. Oral Cytokine Gene Therapy against Murine Tumor Using Attenuated Salmonella Typhimurium. *Int J Cancer* **2001**, *94* (3), 438–443. https://doi.org/10.1002/ijc.1489.

(20) Meng, C.; Chen, Z.; Li, G.; Welte, T.; Shen, H. Nanoplatforms for MRNA Therapeutics. *Advanced Therapeutics*. 2021. https://doi.org/10.1002/adtp.202000099.

(21) Parvin, N.; Joo, S. W.; Mandal, T. K. Enhancing Vaccine Efficacy and Stability: A Review of the Utilization of Nanoparticles in MRNA Vaccines. *Biomolecules* **2024**, *14* (8). https://doi.org/10.3390/biom14081036.

(22) Schoenmaker, L.; Witzigmann, D.; Kulkarni, J. A.; Verbeke, R.; Kersten, G.; Jiskoot, W.; Crommelin, D. J. A. MRNA-Lipid Nanoparticle COVID-19 Vaccines: Structure and Stability. *Int J Pharm* **2021**, *601*, 120586. https://doi.org/10.1016/j.ijpharm.2021.120586.

(23) Smith, S. A.; Selby, L. I.; Johnston, A. P. R.; Such, G. K. The Endosomal Escape of Nanoparticles: Toward More Efficient Cellular Delivery. *Bioconjug Chem* **2019**, *30* (2), 263–272. https://doi.org/10.1021/acs.bioconjchem.8b00732.

(24) Gudlur, S.; Sukthankar, P.; Gao, J.; Avila, L. A.; Hiromasa, Y.; Chen, J.; Iwamoto, T.; Tomich, J. M. Peptide Nanovesicles Formed by the Self-Assembly of Branched

Amphiphilic Peptides. *PLoS One* **2012**, *7* (9). https://doi.org/10.1371/journal.pone.0045374.

(25) Sukthankar, P.; Gudlur, S.; Avila, L. A.; Whitaker, S. K.; Katz, B. B.; Hiromasa, Y.; Gao, J.; Thapa, P.; Moore, D.; Iwamoto, T.; Chen, J.; Tomich, J. M. Branched Oligopeptides Form Nanocapsules with Lipid Vesicle Characteristics. *Langmuir* **2013**. https://doi.org/10.1021/la403492n.

(26) Sukthankar, P.; Whitaker, S. K.; Garcia, M.; Herrera, A.; Boatwright, M.; Prakash, O.; Tomich, J. M. Thermally Induced Conformational Transitions in Nascent Branched Amphiphilic Peptide Capsules. *Langmuir* **2015**. https://doi.org/10.1021/la504381y.

(27) Jia, Z.; Whitaker, S. K.; Tomich, J. M.; Chen, J. Organization and Structure of Branched Amphipathic Oligopeptide Bilayers. *Langmuir* **2016**. https://doi.org/10.1021/acs.langmuir.6b02421.

(28) Barros, S. M.; Whitaker, S. K.; Sukthankar, P.; Avila, L. A.; Gudlur, S.; Warner, M.; Beltrão, E. I. C.; Tomich, J. M. A Review of Solute Encapsulating Nanoparticles Used as Delivery Systems with Emphasis on Branched Amphipathic Peptide Capsules. *Archives of Biochemistry and Biophysics*. 2016. https://doi.org/10.1016/j.abb.2016.02.027.

(29) Sukthankar, P.; Avila, L. A.; Whitaker, S. K.; Iwamoto, T.; Morgenstern, A.; Apostolidis, C.; Liu, K.; Hanzlik, R. P.; Dadachova, E.; Tomich, J. M. Branched Amphiphilic Peptide Capsules: Cellular Uptake and Retention of Encapsulated Solutes. *Biochim Biophys Acta Biomembr* **2014**. https://doi.org/10.1016/j.bbamem.2014.02.005.

(30) Avila, L. A.; Aps, L. R. M. M.; Sukthankar, P.; Ploscariu, N.; Gudlur, S.; Šimo, L.; Szoszkiewicz, R.; Park, Y.; Lee, S. Y.; Iwamoto, T.; Ferreira, L. C. S.; Tomich, J. M.; Avila, L. A.; Aps, L. R. M. M.; Sukthankar, P.; Ploscariu, N.; Gudlur, S.; Šimo, L.; Szoszkiewicz, R.; Park, Y.; Lee, S. Y.; Iwamoto, T.; Ferreira, L. C. S.; Tomich, J. M.; Avila, L. A.; Aps, L. R. M. M.; Sukthankar, P.; Ploscariu, N.; Gudlur, S.; Šimo, L.; Szoszkiewicz, R.; Park, Y.; Lee, S. Y.; Iwamoto, T.; Ferreira, L. C. S.; Tomich, J. M. Branched Amphiphilic Cationic Oligopeptides Form Peptiplexes with DNA: A Study of Their Biophysical Properties and Transfection Efficiency. *Mol Pharm* **2015**, *12* (3), 706–715. https://doi.org/10.1021/mp500524s.

(31) Avila, L. A.; Aps, L. R. M. M.; Ploscariu, N.; Sukthankar, P.; Guo, R.; Wilkinson, K. E.; Games, P.; Szoszkiewicz, R.; Alves, R. P. S.; Diniz, M. O.; Fang, Y.; Ferreira, L. C. S.; Tomich, J. M. Gene Delivery and Immunomodulatory Effects of Plasmid DNA Associated with Branched Amphiphilic Peptide Capsules. *J Control Release* **2016**, *241*, 15–24. https://doi.org/10.1016/j.jconrel.2016.08.042.

(32) Kunte, N.; Westerfield, M.; McGraw, E.; Choi, J.; Akinsipe, T.; Whitaker, S. K.; Brannen, A.; Panizzi, P.; Tomich, J. M.; Avila, L. A. Evaluation of Transfection Efficacy, Biodistribution, and Toxicity of Branched Amphiphilic Peptide Capsules (BAPCs) Associated with MRNA. *Biomater Sci* **2022**. https://doi.org/10.1039/d2bm01314b.

(33) Mcgraw, E.; Roberts, J. D.; Held, D. Insight Into Cellular Uptake and Transcytosis of Peptide Nanoparticles in a Generalist Caterpillar . 1–16.

(34) Avila, L. A.; Chandrasekar, R.; Wilkinson, K. E.; Balthazor, J.; Heerman, M.; Bechard, J.; Brown, S.; Park, Y.; Dhar, S.; Reeck, G. R.; Tomich, J. M. Delivery of Lethal DsRNAs in Insect Diets by Branched Amphiphilic Peptide Capsules. *Journal of Controlled Release* **2018**, *273*, 139–146. https://doi.org/10.1016/j.jconrel.2018.01.010.

(35) Nitish Sunil Kunte. Branched Amphiphilic Peptide Capsules (BAPCs): A Promising Platform for MRNA Therapeutics Delivery., Auburn, Auburn, 2023.

(36) Aditya Prakash Sarode* and Shraddha Dingare. Solid Phase Peptide Synthesis and Its Applications in Tackling Antimicrobial Resistance. *J Antimicrob Agents* **2023**.

(37) Mant, C. T.; Chen, Y.; Yan, Z.; Popa, T. V; Kovacs, J. M.; Mills, J. B.; Tripet, B. P.; Hodges, R. S. HPLC Analysis and Purification of Peptides. *Methods Mol Biol* **2007**, *386*, 3–55. https://doi.org/10.1007/978-1-59745-430-8_1.

(38) Fields, C. G.; Lloyd, D. H.; Macdonald, R. L.; Otteson, K. M.; Noble, R. L. HBTU Activation for Automated Fmoc Solid-Phase Peptide Synthesis. *Pept Res* **1991**, *4* (2), 95–101.

(39) Stathopoulos, P.; Papas, S.; Tsikaris, V. C-TerminalN-Alkylated Peptide Amides Resulting from the Linker Decomposition of the Rink Amide Resin. A New Cleavage Mixture Prevents Their Formation. *Journal of Peptide Science* **2006**, *12* (3), 227–232. https://doi.org/10.1002/psc.706.

(40) Christian Heuer, P. H. G. M. A. S.-M. Scale up in Preparative Chromatography. *J Chromatogr A* **1996**, *752* (1–2), 19–29.

(41) Pardi, N.; Hogan, M. J.; Porter, F. W.; Weissman, D. MRNA Vaccines-a New Era in Vaccinology. *Nature Reviews Drug Discovery*. 2018. https://doi.org/10.1038/nrd.2017.243.

(42) Pulendran, B.; Ahmed, R. Immunological Mechanisms of Vaccination. *Nature Immunology*. 2011. https://doi.org/10.1038/ni.2039.

(43) Bettini, E.; Locci, M. SARS-CoV-2 MRNA Vaccines: Immunological Mechanism and Beyond. *Vaccines (Basel)* **2021**, *9* (2). https://doi.org/10.3390/vaccines9020147.

(44) Song, Z.; Jin, L.; Jiao, L.; Yu, R.; Liu, H.; Zhang, S.; Hu, Y.; Sun, Y.; Li, E.; Zhao, G.; Liu, Z.; Cai, T. ALC-0315 Lipid-Based MRNA LNP Induces Stronger Cellular Immune Responses Postvaccination. *Mol Pharm* **2025**, *22* (2), 859–870. https://doi.org/10.1021/acs.molpharmaceut.4c00995.

(45) Xuan, L.; Ju, Z.; Skonieczna, M.; Zhou, P.-K.; Huang, R. Nanoparticles-Induced Potential Toxicity on Human Health: Applications, Toxicity Mechanisms, and Evaluation Models. *MedComm (Beijing)* **2023**, *4* (4), e327. https://doi.org/10.1002/mco2.327.

(46) Bahadar, H.; Maqbool, F.; Niaz, K.; Abdollahi, M. Toxicity of Nanoparticles and an Overview of Current Experimental Models. *Iran Biomed J* **2016**, *20* (1), 1–11. https://doi.org/10.7508/ibj.2016.01.001.

(47) Chen, J.; Hessler, J. A.; Putchakayala, K.; Panama, B. K.; Khan, D. P.; Hong, S.; Mullen, D. G.; Dimaggio, S. C.; Som, A.; Tew, G. N.; Lopatin, A. N.; Baker, J. R.; Holl, M. M. B.; Orr, B. G. Cationic Nanoparticles Induce Nanoscale Disruption in Living Cell Plasma Membranes. *J Phys Chem B* **2009**, *113* (32), 11179–11185. https://doi.org/10.1021/jp9033936.

(48) Cui, S.; Wang, Y.; Gong, Y.; Lin, X.; Zhao, Y.; Zhi, D.; Zhou, Q.; Zhang, S. Correlation of the Cytotoxic Effects of Cationic Lipids with Their Headgroups. *Toxicol Res (Camb)* **2018**, *7* (3), 473–479. https://doi.org/10.1039/c8tx00005k.

(49) Barros, S. D. M.; Avila, L. A.; Whitaker, S. K.; Wilkinson, K. E.; Sukthankar, P.; Beltrão, E. I. C.; Tomich, J. M. Branched Amphipathic Peptide Capsules: Different Ratios of the Two Constituent Peptides Direct Distinct Bilayer Structures, Sizes, and DNA Transfection Efficiency. *Langmuir* **2017**. https://doi.org/10.1021/acs.langmuir.7b00912.

(50) Mohammadinejad, R.; Moosavi, M. A.; Tavakol, S.; Vardar, D. Ö.; Hosseini, A.; Rahmati, M.; Dini, L.; Hussain, S.; Mandegary, A.; Klionsky, D. J. Necrotic, Apoptotic and Autophagic Cell Fates Triggered by Nanoparticles. *Autophagy* **2019**, *15* (1), 4–33. https://doi.org/10.1080/15548627.2018.1509171.

(51) Julien, O.; Wells, J. A. Caspases and Their Substrates. *Cell Death Differ* **2017**, *24* (8), 1380–1389. https://doi.org/10.1038/cdd.2017.44.

(52) Chen, Y. S.; Hung, Y. C.; Liau, I.; Huang, G. S. Assessment of the in Vivo Toxicity of Gold Nanoparticles. *Nanoscale Res Lett* **2009**. https://doi.org/10.1007/s11671-009-9334-6.

(53) Abdal Dayem, A.; Hossain, M.; Lee, S.; Kim, K.; Saha, S.; Yang, G.-M.; Choi, H.; Cho, S.-G. The Role of Reactive Oxygen Species (ROS) in the Biological Activities of Metallic Nanoparticles. *Int J Mol Sci* **2017**, *18* (1), 120. https://doi.org/10.3390/ijms18010120.

(54) JAN FROUZ, R. J. L. A. Y. A. A. LARVAL GUT PH PROFILE IN PESTIFEROUS CHIRONOMUSCRASSICAUDATUS AND GLYPTOTENDIPES PARIPES (CHIRONOMIDAE: DIPTERA) IN REFERENCE TO THE TOXICITY POTENTIAL OF BACILLUS THURINGIENSIS SEROVAR ISRAELENSIS. *J. of the American Mosquito Control Association* **2007**, *23* (3), 355–358.

Appendix

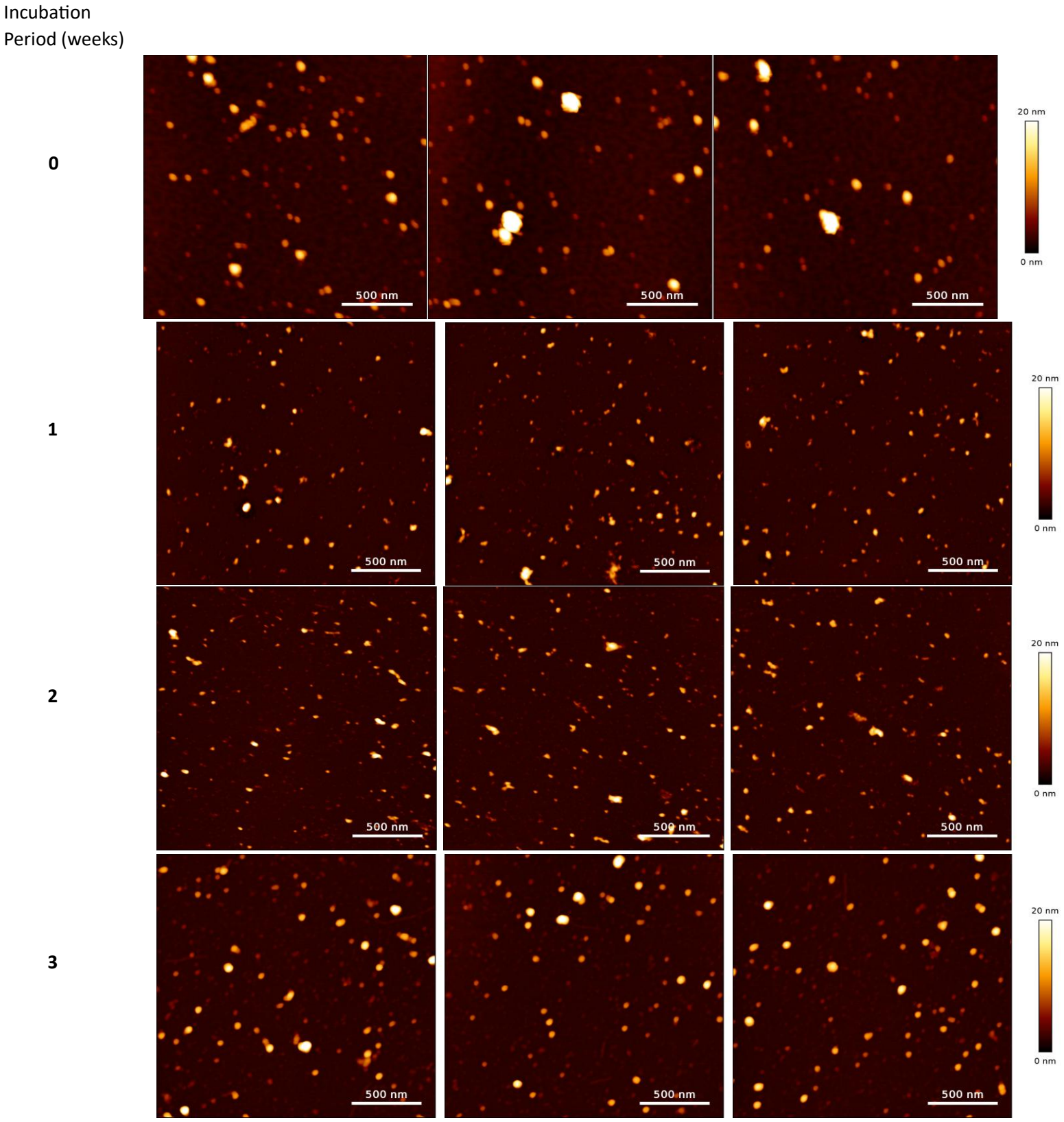

Supplementary Figure 1: AFM Images. BAPC+mRNA 0, 1, 2, 3-Week Incubation.

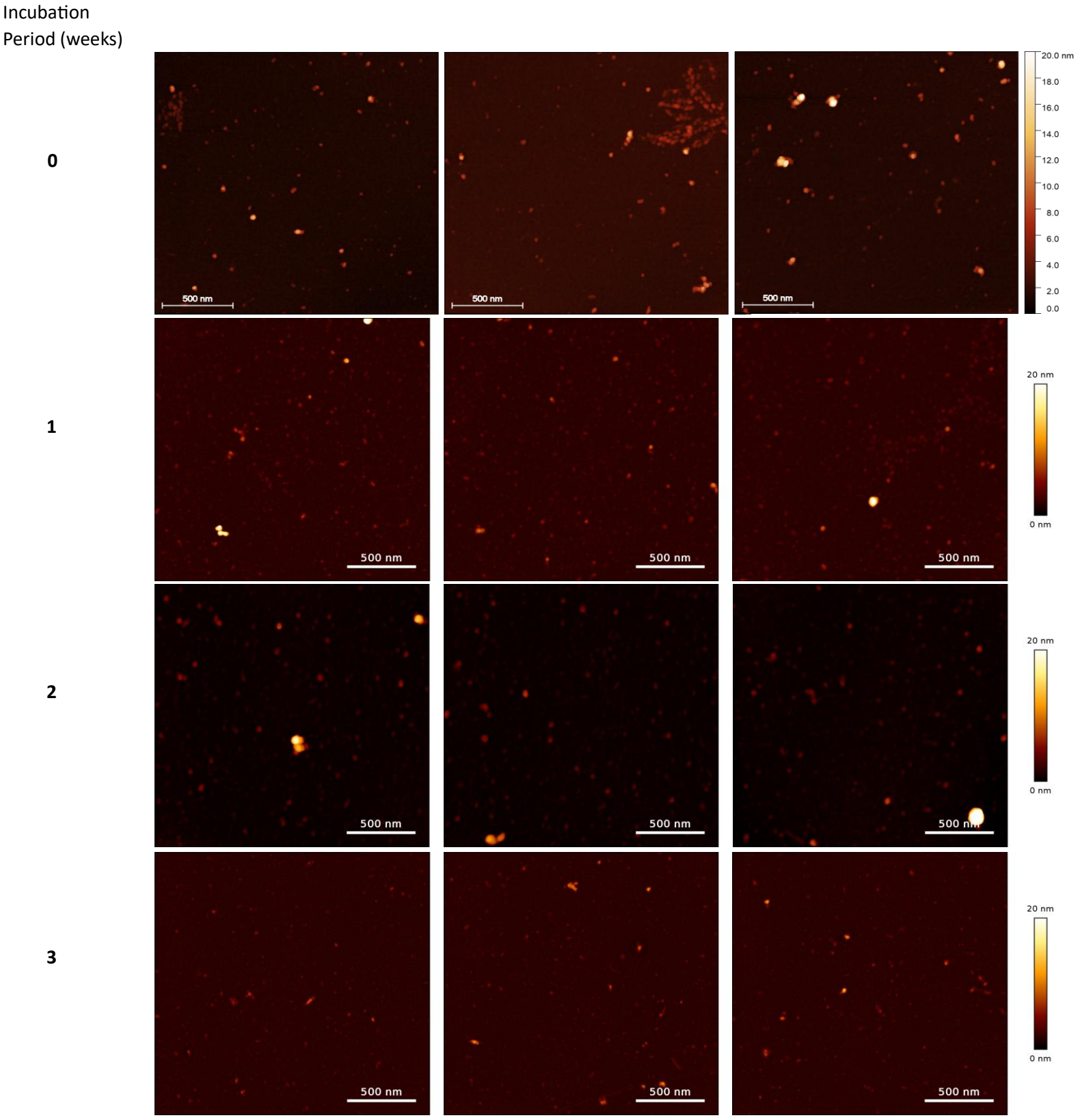

Supplementary Figure 2: AFM Images. BAPC 0, 1, 2, 3-Week Incubation.

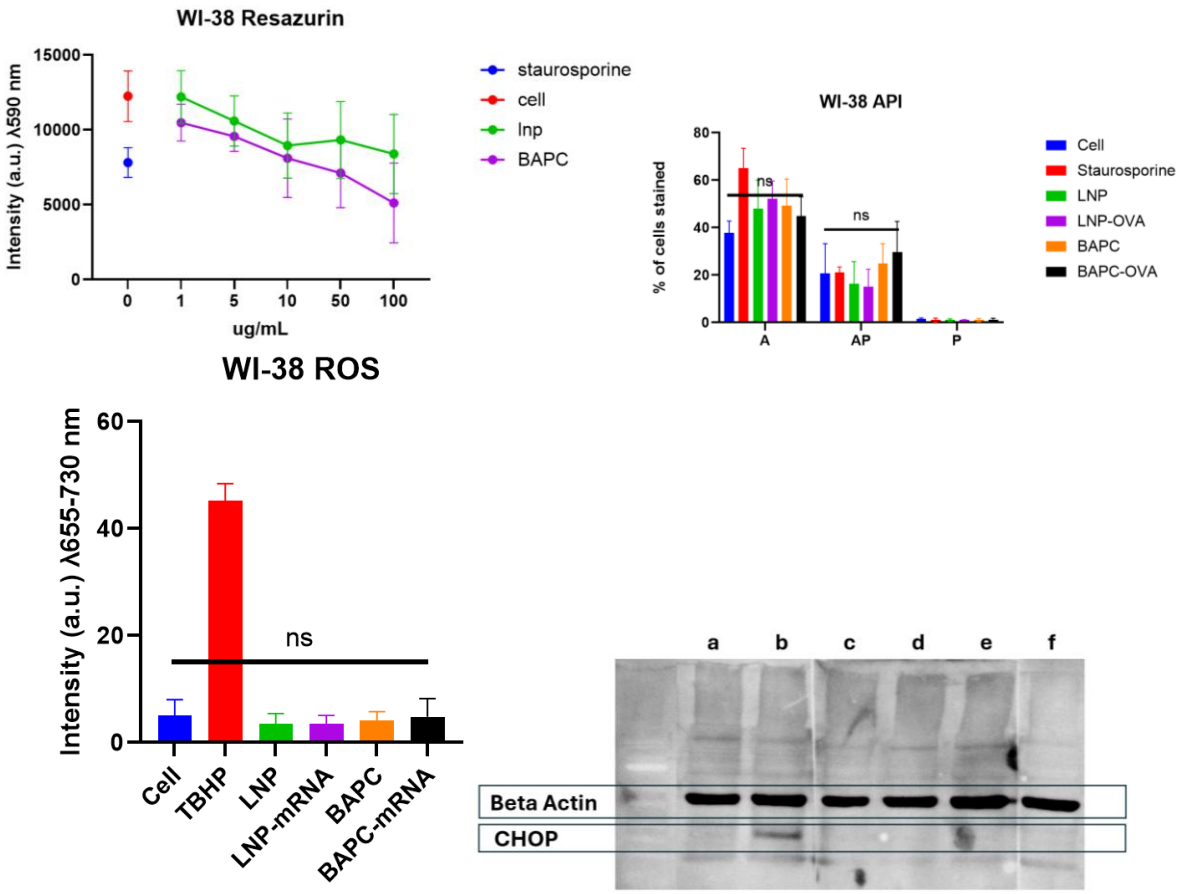

Supplementary Figure 3: Assessment of *in vitro* toxicity. Acute toxicity induced in WI-38 fibroblasts by 24h incubation with 10 µg/mL BAPC-mRNA or LNP-mRNA Complexes. (A) Resazurin Assay. (B) Annexin/PI apoptosis/necrosis staining. (C) Total ROS generation. (D) CHOP/DDIT3 activation. Non-statistical significance (ns) was considered when $p > 0.05$.

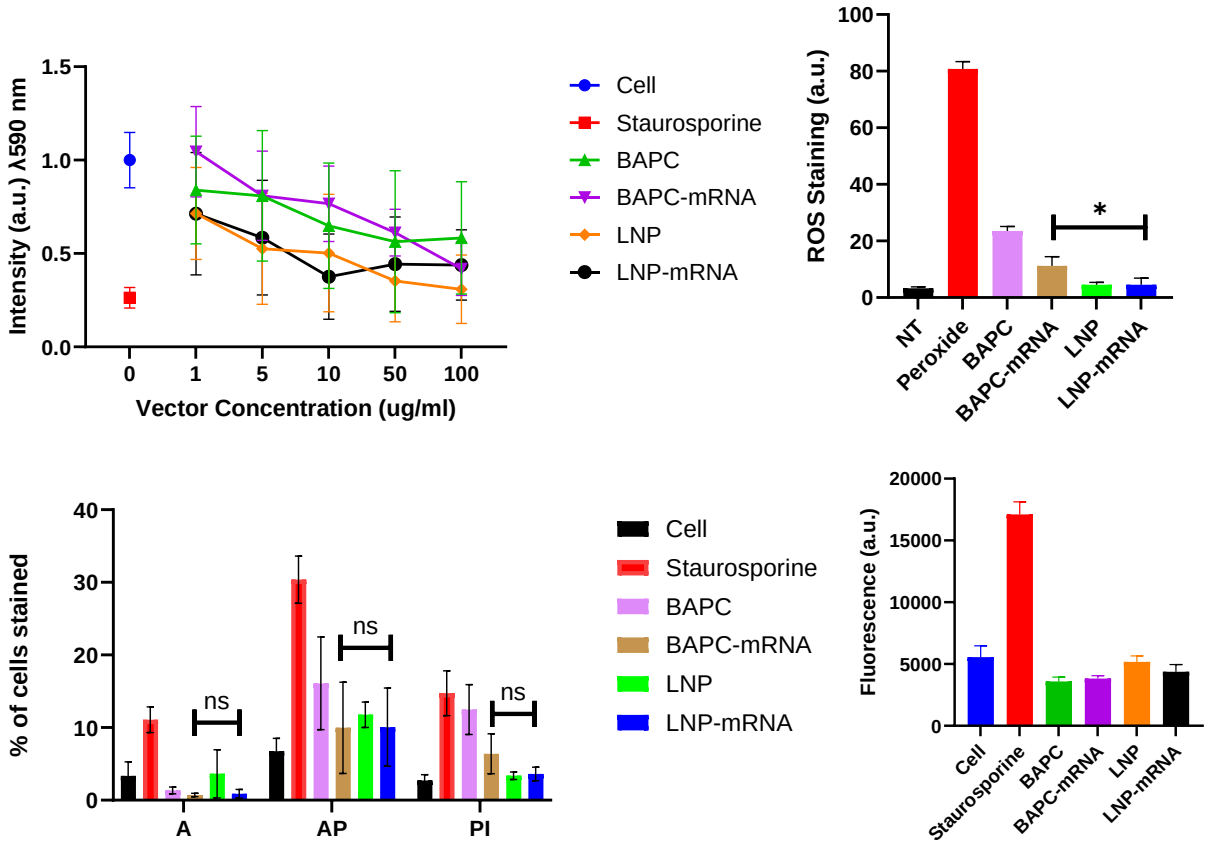

Supplementary Figure 4: Assessment of *in vitro* toxicity. Acute toxicity induced in Chinese Hamster Ovary cells by 24h incubation with 10 µg/mL BAPC-mRNA or LNP-mRNA Complexes. (A) Resazurin Assay. (B) Total ROS generation. (C) Annexin/PI apoptosis/necrosis staining. (D) Caspase 3/7 activation. Non-statistical significance (ns) was considered when $p > 0.05$, (*) $p < 0.01$.

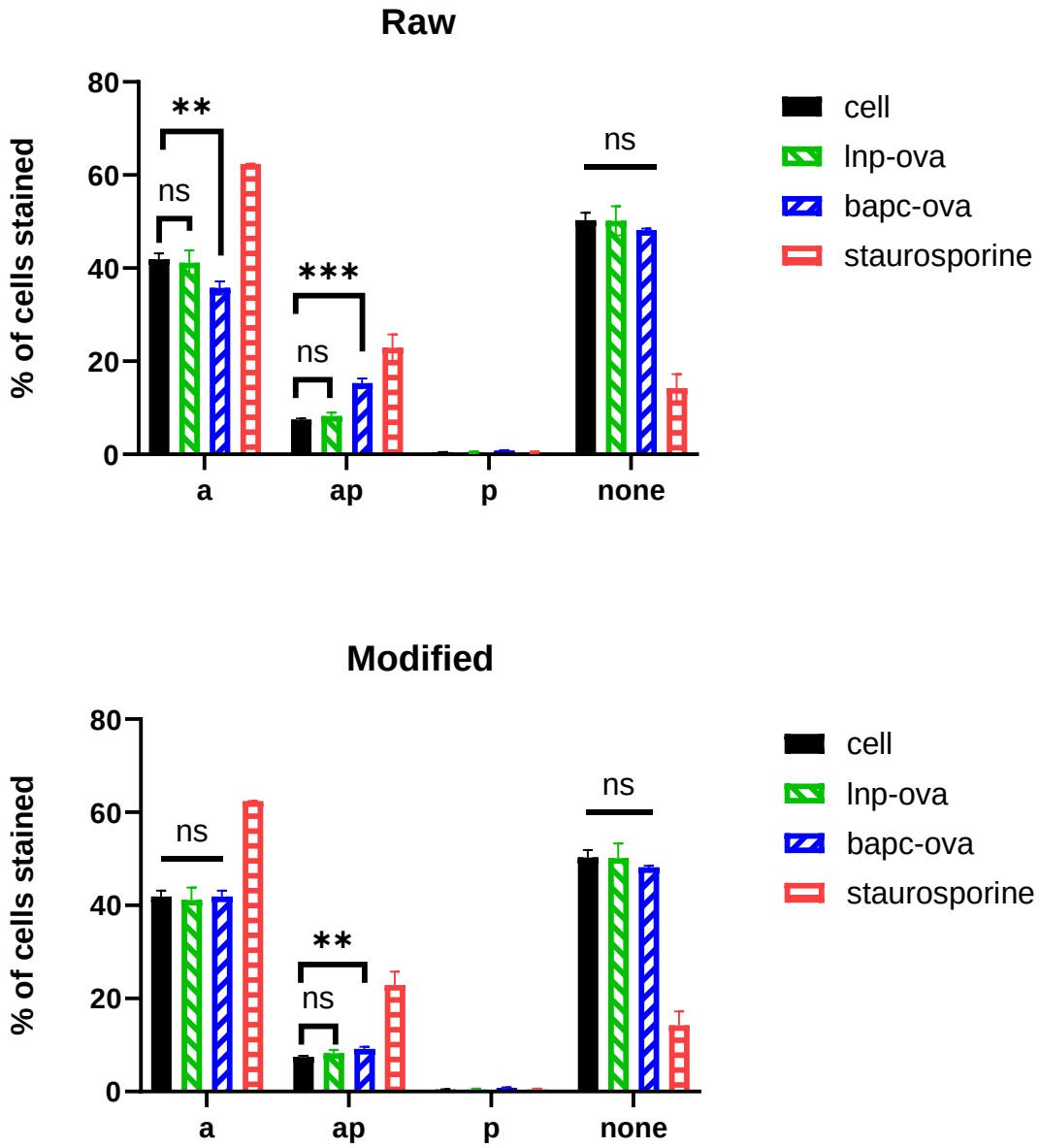

Supplementary Figure 5: RAMOS Annexin/PI Staining. Acute toxicity induced by 24h incubation with 10 µg/mL BAPC-mRNA or LNP-mRNA Complexes in a RAMOS suspension cells. (**) $p < 0.001$, (***) $p < 0.001$. Non-statistical significance (ns) was considered when $p > 0.05$.

a = annexin staining

ap = annexin/pi staining

p = pi staining

None = no staining

In the raw graph in Supp. Fig. 5, we can see that annexin/pi double stained cells may originate from an already apoptotic population of cells. Modifying a second graph to shift percentages

from the BAPC-ova ap population and match the average BAPC annexin only population to that of the cell annexin only population helps to show that there is a minimal increase of healthy cells being turned apoptotic and necrotic (ap stained) after treatment with BAPC-OVA mRNA complexes.

Modified = Raw ap – (cell a average – bapc a); bapc a = cell a

RAMOS cultures as were kept in our lab often contained many old and apoptotic cells from previous passages due to a lack of available methods for their removal between passages. BAPC-mRNA complexes may have expedited cell death in these already weekend or apoptotic cells.